Electronic Supplementary Materials

Hypothetical Binodal Zeolitic Frameworks

Alexandra Simperler,[a] Martin D. Foster,[a] Olaf Delgado Friedrichs,[b] Robert G. Bell,[a]* Filipe A. Almeida Paz,[c,d] and Jacek Klinowski[c]*

[a]Davy-Faraday Research Laboratory, The Royal Institution of Great Britain, 21 Albemarle Street, London W1S 4BS, U.K.

[b]Wilhelm Schickard Institut für Informatik und ZBIT Zentrum für Bioinformatik, Universität Tübingen, Sand 14, D-72072 Tübingen, Germany.

[c]Department of Chemistry, University of Cambridge, Lensfield Road, Cambridge, CB2 1EW, U.K.

[d]Department of Chemistry, CICECO, University of Aveiro, Campus Universitário de Santiago, Aveiro, 3810-193, Portugal.

Summary. Hypothetical binodal zeolitic structures (structures containing two kinds of tetrahedral sites) were systematically enumerated using tiling theory and characterised by computational chemistry methods. Each of the 109 refineable topologies based on "simple tilings" was converted into a silica polymorph, and its energy minimised using the GULP program with the Sanders-Catlow silica potential. Optimised structural parameters, framework energies relative to α-quartz and volumes accessible to sorption have been calculated. 11 of the 30 known binodal topologies listed in the Atlas of Zeolite Framework Types were found, leaving 98 unknown topologies. The chemical feasibility of each structure as a zeolite was evaluated by means of a feasibility factor derived from the correlation between lattice energy and framework density. Structures are described using a model-building approach, and are divided into 15 families, based on common structural features. Many "feasible" structures contain only small pores. Several very open structures were also enumerated, although they contain 3-membered rings which are thermodynamically disfavoured and not found in conventional zeolites.

* To whom correspondence should be addressed. E-mail: rob@ri.ac.uk (RGB) and jk18@cam.ac.uk (JK).

We believe that such topologies may be realizeable as framework materials, but with different elemental compositions to those normally associated with zeolites.

Key words: tiling theory, enumeration, zeolites, hypothetical structures

Introduction

Zeolites find many important applications in science and technology in areas as diverse as catalysis, chemical separation, water softening, agriculture, refrigeration and opto-electronics. 152 distinct structural types of zeolites have now been identified (Baerlocher, et al. 2001). Unusually, the definition of a zeolite is based not on chemical composition or function, but rather on atomic-scale geometry. In order to qualify as a zeolite or zeolite-type material (zeotype), a mineral or synthetic material must possess a framework composed of corner-sharing tetrahedra. There is an additional requirement of "openness", simultaneously dependent on density and smallest ring size, thus excluding denser minerals. Another way of expressing this is in terms of a 4-connected net in which each vertex, in chemical terms the central atom of a tetrahedron, is connected to its four closest neighbours, normally via an oxygen bridge.

The enumeration of hypothetical zeolitic framework structures (Klinowski 1998) is of considerable scientific and practical interest in terms of generating new nanoporous architectures. Enumeration originates with the work of Wells (Wells 1977; 1979; 1984) on three-dimensional nets and polyhedra. Smith and collaborators (Smith 1988; 1993), Alberti (Alberti 1979), Sato (Sato 1984; 1987), Sherman and Bennett (Sherman & Bennett 1973), Barrer and Villiger (Barrer & Villiger 1969), O'Keeffe and collaborators (Boisen, et al. 1999; O'Keeffe & Hyde 1996b; O'Keeffe & Hyde 1996a) and Akporiaye and Price (Akporiaye & Price 1989) found many possible new structures by combining various structural subunits. More recent work involves computer search algorithms (Boisen, et al. 1999; Foster & Treacy 2004; Mellot-Draznieks, et al. 2000; Treacy, et al. 1997).

Our work is based on advances in combinatorial tiling theory (Dress, et al. 1993). A tiling is a periodic subdivision of three-dimensional space into connected regions, which we call *tiles*. If two tiles meet along a surface, the surface is called a *face*. If three or more faces meet along a curve, we call the curve an *edge*. If at least three edges meet at a point, we call that point a *vertex*. A network is thus formed by the vertices and edges. The configuration of edges, faces and tiles around a given vertex can be

described via the so-called vertex figure, obtained by placing the centre of a small notational sphere at the vertex and considering the tiling of that sphere formed by the intersections with the different tiles touching that vertex. We have already enumerated all possible Euclidean uni-, bi- and trinodal tilings based on simple vertex figures and all uninodal tilings with vertex figures containing up to six extra edges (Delgado Friedrichs 2001), and the computer program used for this task is available from the authors upon request (delgado@informatik.uni-tuebingen.de).

The tiling approach identified networks with 1, 2, and 3 kinds of inequivalent vertices, which we call uninodal, binodal and trinodal (Delgado Friedrichs, et al. 1999). We have shown that there are exactly 9, 117 and 926 topological types of 4-connected uninodal, binodal and trinodal nets, respectively, which are based on "simple" periodic tilings (as explained in ref. (Delgado Friedrichs, et al. 1999)). In addition, there are at least 157 additional uninodal nets derived from "quasi-simple" tilings (the vertex figures of which are derived from tetrahedra, but contain double edges) (Delgado Friedrichs, et al. 1999) and which have already been discussed elsewhere (Foster, et al. 2001; Foster, et al. 2003; Foster, et al. 2004a; Foster, et al. 2004b; Simperler, et al. 2004). For example, zeolitic structure types SOD, LTA, RHO, FAU, KFI and CHA are all based on quasi-simple tilings. An example of a non-simple tiling is that of GIS, where the tile has some two-connected vertices.

Here we focus our attention on the binodal structures, i.e., those with two topologically inequivalent types of tetrahedral vertex (T-atom sites) derived only from simple tilings, meaning that they can be readily described by the packing of convex polyhedra, the vertices of which are all three-connected. Structures containing cages are thus found in abundance, while those with, for instance, more "cylindrical" channels are less common, and tend to have lower framework density than the "quasi-simple" structures, with a greater proportion lying in the range of density where most known zeolites are found, as opposed to denser minerals. On the other hand, many of the known zeolite structure types cannot be constructed from simple tilings. Thus, simple tilings cannot therefore generate the complete set of binodal zeolites. Seven of the 21 known *uninodal* zeolites correspond to simple tilings, and the remaining 14, together with several mineral structures (although not quartz) are constructed using quasi-simple tilings. We have found 11 of the 30 known binodal zeolite types, and the remaining 19 will be found by considering quasi-simple tilings, just as with the uninodal structures. The number of potential binodal networks thus generated will be enormous, and their enumeration will require the use of a state-of-the-art

computational facilities. However, only very few binodal structures have previously been enumerated, while nearly all uninodal structures derived from the tilings were previously known, either as crystal structures, or as hypothetical nets. It is therefore of interest to describe the binodal structures derived from simple tilings only.

To characterise the structures, we follow procedures to identical those used in our previous work (Foster, et al. 2003; Foster, et al. 2004b). This involves generating model SiO_2 polymorphs from the tiling nets, and optimising them using lattice energy minimisation. Apart from obtaining an optimised structure for each topology, we also calculate a lattice energy, which provides an accurate guide to the thermodynamic stability that such a phase might have. A "feasibility factor", ϑ, derived from the correlation between lattice energy and density calculated for known zeolite structure types, serves as a further measure of thermodynamic feasibility. We have also calculated the accessible volume for each pore system using a standard definition (Cerius^2 1999).

In describing the structural characteristics of each framework, we have resorted to the "model building" approach (Baerlocher, et al. 2001; Liebau, et al. 1986; Meier 1986; Smith 1988), which is consistent with descriptions found in the online zeolite database, and allows structures to be classified into "families" if they share certain structural motifs. As part of this analysis we define as a composite building unit (CBU) every small finite unit from which a structure may be generated. These can be corner-, edge-, or face-sharing, or joined to one another by single linkages. The automated assembly of such units is also a potential method of structural enumeration, as demonstrated by Mellot-Draznieks et al. (Mellot-Draznieks, et al. 2002; Mellot-Draznieks, et al. 2000). Zeolite structures may also be described in terms of the strictly defined secondary building units (SBUs), one type of which may be used to build a unit cell of the zeolite, without any sharing of T-atoms. Here, we have not used the SBU approach, finding it more informative to use alternative descriptions (in general our building units tend to be larger). However the SBUs involved may be readily identified, as may the infinite periodic building units (PerBUs). We note that none of the units discussed are intended to represent the precursors from which zeolite crystals grow; neither do they necessarily correspond to the tiles of the original nets.

We discuss the structures in terms of the component units, and relate these to the calculated stability and feasibility. Taken together, thermodynamic feasibilty and the nature of the building units can provide a good initial guide as to which of these structures could be most readily synthesised.

Energy minimisation

The systematically enumerated nets (Delgado Friedrichs, et al. 1999) were first converted into atomistic models. This was done by inserting a Si atom at each vertex point in the network, and placing a bridging oxygen between each pair of adjacent Si atoms. Each net was scaled such that the vertices were separated by about 3.1 Å, a typical Si–Si distance. The resulting structure was then pre-optimised using the DLS (distance least squares) method (Meier & Villiger 1969) which performs geometric refinement of the structure by fitting bond lengths and angles to the prescribed values, and reduces the amount of computer time needed for the subsequent minimisation of lattice energy. Its use was found to have no influence on the final result: using lattice energy minimisation from the outset gives the same structure, but at greater computational expense. The lattice energy and crystallographic data are those extracted from the GULP minimisations, whereas coordination sequences, bond distances and angles were calculated with zeoTsites (version 1.2) (Sastre & Gale 2001). The connectivity was additionally checked with software tool KRIBER (version 1.1) (Bialek 1995). Additional calculations were carried out using Cerius^2 (Cerius^2 1999). Structural figures were prepared using GDIS (GDIS 2004) and POV-Ray (POV-Ray 2004). The lattice energy, ΔE_{quartz}, given in Table 1, is relative to that of α-quartz, calculated using the same potential model, and is thus analogous to the heat of transition reported for several high-silica zeolites (Henson, et al. 1994; Hu, et al. 1995; Moloy, et al. 2002; Navrotsky, et al. 1995; Petrovic, et al. 1993; Piccione, et al. 2000; Piccione, et al. 2001; Piccione, et al. 2002).

The Feasibility Factor

The well-established relationship between framework density and calculated lattice energy (Foster, et al. 2001; Foster, et al. 2003; Foster, et al. 2004a; Foster, et al. 2004b; Simperler, et al. 2004) was confirmed experimentally (Henson, et al. 1994) for known zeolites. Using the standard least-squares technique, a straight line was fitted to 145 data points obtained from minimising quartz and all the known zeolite topologies in an purely siliceous form (Figure 1). We excluded the four non-silicate structure types which substantially deviate from the rest: WEI (calcium beryllophosphate), CZP (sodium zincophosphate), OSO (potassium berylosilicate) and RWY (gallium germanium sulphide). The line of best fit has the formula $y = -1.4433x + 40.3904$, where x is framework density (F_D) and y is ΔE_{quartz}. The feasibility factor, ϑ, is then simply the

dimensionless deviation of a data point (x_1, y_1) from the line of best fit, given by the vertical offset $\vartheta = \frac{|1.4433x_1 + y_1 + 40.3904|}{1.4433}$. Being formally independent of the framework density, the feasibility factor ϑ is thus a convenient way of discriminating between candidate structures, and can be compared with the values obtained from known zeolite structures. We minimised all the known zeolite topologies as silica polymorphs, regardless of the actual composition in which they occur, and we believe that ϑ is a better gauge of the feasibility of the structure than ΔE_{quartz} alone, as evidenced by the fact that seven of the ten lowest ϑ values in Table 1 belong to structures with known zeolite topologies. A ranking in order of ascending ΔE_{quartz} would, in contrast, produce only four. Virtually all of the topologies which are known in the form of silicates, aluminosilicates or aluminophosphates, including those with low levels of heteroatom substitution, have $\vartheta < 5$. This reflects the similarity of preferred geometry between (alumino)silicates and AlPOs. The highest values of ϑ are 5.03 for AFY (Co-AlPO-50), which has 19% framework cobalt, and 5.18 for AHT, only known as the thermally unstable material AlPO-H2. By analogy, we define structures with $\vartheta < 5$ as feasible "conventional" zeolites, i.e., those for which natural zeolites along with high-silica and AlPO forms are known. Framework types with more "exotic" compositions have $\vartheta > 5$. For example, the zincosilicates VNI, VSV and RSN have ϑ of 5.75, 6.07 and 6.09, respectively. Beryllosilicates, generally containing 3-rings, also have higher ϑ, e.g. LOV (6.51), NAB (10.99) and OSO (23.30), while the beryllophosphate weinebeneite has $\vartheta = 12.24$ and the zincophosphate CZP $\vartheta = 20.92$. We therefore propose that ϑ values up to 25 indicate that the topology may be feasible in the form of an "oxide" material. Above this, we note that for RWY, the only zeotype structure known solely as a framework sulphide, $\vartheta = 51.69$. Many other compositions, such as metal-organic frameworks, are of course, possible. This means that although a structure may be deemed highly unfeasible as a zeolite, it may exist in other chemical forms. Also, the precise value of ϑ will be an unreliable guide in the high region, since it is based only on a silica model. In order to gauge the feasibility of a particular topology in a different composition, it would be necessary to carry out separate series of computations, taking into account the actual composition.

The Cerius^2 software suite (Cerius^2 1999) was used for visualising and manipulating the structures and for calculating free volumes, space group symmetry and other parameters. In addition to calculating the energetics of the hypothetical structures, it is important to compare the calculated values with the values for all

known zeolite frameworks. Thus all relevant properties were also calculated for the purely siliceous forms of all known zeolite topologies. Lattice energies were calculated relative to α-quartz, the most stable form of the mineral at ambient temperature.

The "available volume", defined as the difference between the volume of the unit cell and the effective volume of all the atoms, depends on the van der Waals radii used for each atom. "Occupiable volume" is the volume which can be occupied by a probe molecule with a given radius as it probes the surface of the structure. The "accessible volume" is determined by tracing out the volume by the centre of the probe molecule as it follows the structure contours, but with the extra requirement that the probe must enter the unit cell from the outside via sufficiently wide pores or channels. The accessible volume gives an indication of the space available within each structure for applications in molecular sieving and catalysis. The calculations of the accessible volume were performed using the Free Volume module of the Cerius^2 package, which applies the Connolly method (Connolly 1985). consisting of "rolling" a probe molecule with a given radius over the van der Waals surface of the framework atoms. We have used a probe molecule with a radius of 1.4 Å (such as water) and 1.32 and 0.9 Å for the radii of O and Si atoms, respectively. The void volume, enclosed within the Connolly surface, was calculated first. The accessible volume was then calculated by requiring the probe molecule to enter the unit cell from the outside.

Results and Discussion

Of the 117 structures, eight could not be optimised, either because refinement was not possible, or because of failure during minimisation, usually resulting in loss of the original network topology. The remaining 109 structures are described below. For the most part, these minimised smoothly without any loss of symmetry, although there are a few whose low-energy symmetry is lower than that of the original space group. In these instances, the original space group is shown in parentheses in Table 2.

Figure 1a-b gives the plot of framework energy relative to α-quartz, E_F, versus the framework density, F_D, for all known zeolites. Relative framework energies of the hypothetical binodal frameworks range from 11.15 kJ mol^{-1} (structure 2_114) to as much as 515.43 kJ mol^{-1} (structure 2_72) (Figure 1c). Figure 1d plots the framework energy versus the framework density for the hypothetical binodal structures with energies

below 30 kJ mol^{-1}, the range considered as the most "desirable", and with framework densities typical of the known zeolites.

Figure 2a gives the plot of accessible volume versus framework density for the known structural types and Figure 2b-c the corresponding plot for hypothetical binodal zeolites. Low framework density structures are of particular interest, as they have very high accessible free volumes. Of the structures with framework densities below 18 Si atoms/1000 $Å^3$, structures 2_57, 2_58, 2_59, 2_82, 2_85, 2_86, 2_87, 2_91, 2_95, 2_96, 2_102, 2_103, 2_106, 2_108, 2_109, 2_110, 2_112, 2_113, 2_114, 2_117 are energetically stable (Figure 1c). Many hypothetical structures have dense frameworks, which are largely inaccessible. However, as many known zeolite topologies have low accessible volumes (Figure 2a), a structure cannot be ruled out as a feasible topology on the basis of the low accessible free volume, even though it may be of no interest to sorption, ion exchange or catalysis. A plot of framework density for known zeolites and for dense silicate frameworks against the size of the smallest ring in the structure (Brunner & Meier 1989), shows that very open frameworks with low F_D have the largest number of 4- and 3-membered rings, and that there is a gap in F_D between compact minerals, such as quartz and tridymite, and the zeolite frameworks. The lower boundary of F_D for known zeolites is from about 11 tetrahedral atoms per 1000 $Å^3$ in materials with 4-membered rings to about 17 tetrahedral atoms in materials with 5+ rings, where the plus sign signifies that some tetrahedral atoms are associated only with the larger rings.

Figure 3 plots the framework energy with respect to α-quartz for the known zeolitic structures and the hypothetical binodal structures versus the accessible volume, thus combining information contained in Figures 1 and 2. Structures of the greatest practical interest are those with low energies and large volumes (see inset in Figure 3b). Full details of all the structures have been recently published elsewhere (Foster, et al. 2004b). Crystallographic CIF files from which powder X-ray diffraction patterns can be easily calculated are given in Supplementary Information.

The structures have been divided into fifteen families, the members of which share a common building scheme or structural unit. As explained above, the building units used do not necessarily equate to SBUs or PerBUs in the strict sense. We also note that the allocation of a structure to a certain family is not unequivocal: there are several structures which could equally belong to more than one family. The order in which the various families are discussed is dictated by the feasibility factor of the most feasible structure in that family. Members of a particular family are shown in Figures 4-18 in the same order. The more feasible structures will thus be encountered earlier in the

following sections, with the exception of the "orphan family" which contains several chemically feasible members. In describing the various structures, we use standard nomenclature from the zeolite literature. For instance, "D6R" refers to a double six-ring unit. In describing polyhedral cages or units, the [M^xN^y] system adopted by Smith (Smith 1988) is also used, where (*M, N*) is the number of edges defining a given face and (*x, y*) is the number of times that face appears in the polyhedron. Results are also tabulated in Table 1 (in order of ϑ) and Table 2 (in numerical order of the structures). Table 1 gives ϑ, ΔE_{quartz}, the framework density and the coordination sequences of the T-sites. Table 2 gives the crystallographic data.

ABC-6 family

Of the 109 refinable binodal structures, thirteen (2_87, 2_89, 2_84, 2_90, 2_86, 2_83, 2_107, 2_110, 2_106, 2_108, 2_78, 2_40 and 2_33), can be described using the building scheme for the ABC-6 family (van Koningsveld 2004). Six of these are known frameworks: 2_89 = ERI, 2_84 = EAB, 2_90 = SAT, 2_83 = LEV, 2_107 = LOS and 2_78 = AFX. The PerBU of the family consists of a hexagonal array of isolated 6-membered rings, which are related by pure translations along (100) and (010). A three letter code (A, B, and C) gives the connection mode of the layers along (001). The 6-membered rings of A are centred at (0,0), while layer B is shifted by (+2/3*a*,+1/3*b*) and layer C by (+1/3*a*,+2/3b). Connection between 6-rings in adjacent layers is invariably via 4-rings. In (001) projection, there is a close similarity between all the structures of this family, epitomized by that of 2_106 (Figure 4a), where the hexagonal array of 6-rings, interspersed by 4-rings, is clearly evident. Each structure is uniquely characterised by its (001) stacking sequence, and these sequences are also illustrated in Figure 4 in projections of the unit cells perpendicular to (001). The stacking sequences of the 13 structures (in order of their "thermodynamic feasibility") are ABBACBBC(A) for 2_87 (Figure 4b), ACAABA(A) for 2_89 (ERI) (Figure 4d), ACCABB(A) for 2_84 (EAB) (Figure 4e), AABABBCBCCAC(A) for 2_90 (SAT) (Figure 4f), ABBC(A) for 2_86 (Figure 4g), AACBBACCB(A) for 2_83 (LEV) (Figure 4i), ABAC(A) for 2_107 (LOS) (Figure 4j), ACABABCBC(A) for 2_110 (Figure 4k), ACABCB(A) for 2_106 (Figure 4l), ACACBABACBCB(A) for 2_108 (Figure 4m), ACCAABBA(A) for 2_78 (AFX) (Figure 4n), ACCCBBBAA(A) for 2_40 (Figure 4o), and AAAACCCCBBBB(A) for 2_33 (Figure 4q). 2_87, 2_89, 2_84, 2_107, 2_106 and 2_78, have hexagonal symmetry, space group $P6_3/mmc$, while 2_90, 2_83, 2_110, 2_108, 2_40 and 2_33 (all *R*-3m) and 2_86 (*P*-3m1) are trigonal. The ABC-6 structures, both known and hypothetical, are among the most

thermodynamically favoured as silica polymorphs and, as can be seen from Table 1, have high chemical feasibilities ($0.08 < \vartheta < 0.98$) except for 2_40 and 2_33, which have ϑ of 14.97 and 20.83, respectively. In terms of their pore structures, 2_110, 2_106 and 2_108 have cages only accessible through 6-rings. In contrast, 2_87, 2_86 and 2_78 possess 8-rings as the maximum pore. The ABC-6 structures may also be thought of in terms of stacks, or chains, of cages linked parallel to the (001) direction though 6-rings and, depending on symmetry, there are either one or two distinct types of stack. For example, the most feasible structure 2_87 contains both the [$4^9 6^2 8^3$] gmelinite cages, and [$4^9 6^8 8^3$] EAB cages. In contrast to the case of EAB, where these cages are in different (001) stacks, in 2_87 they alternate along (001) (Figure 4c). Parallel to these are stacks of alternating sodalite cages and double 6-rings (D6R). 2_83 also has the alternating chains of D6R and sodalite cages, but parallel to these are stacks only containing LEV cages (Figure 4h). The less dense structures 2_40 and 2_33 are interesting, as they have large cages linked through elongated 10 and 12-rings, respectively (Figure 4p and 4r). However, these structures are less stable, containing stacks of two and three D6R, respectively, linked though shared 6-rings.

[$3^2 5^6$] family

Four structures (2_103, 2_55, 2_56 and 2_104) are built up from columns of [$3^2 5^6$] polyhedral units (Figure 5b) arranged hexagonally so as to give 12-membered ring channels along the *c* direction (Figure 5a). In the most stable framework, 2_103 (Figure 5a-c), the [$3^2 5^6$] units are linked by sharing their "terminal" 3-membered ring windows (Figure 5c), with each alternate unit related to its neighbour by a 180° reflection. Structure 2_55 has these small cage units separated by a [$3^2 4^3$] unit (i.e., a trigonal prism, or D3R) (Figure 5d), with the large channels cross-linked via elongated 8-rings. 2_56 and 2_104 (Figure 5e-f) are distorted counterparts of 2_55 and 2_103, respectively. In these trigonal structures, the distortion of the building units arises from the lack of alternation along *z*, entailing a "twist" of the units in order to ensure that the 3-rings remain eclipsed. The distortion is slightly smaller in 2_56 due to the interposition of the D3R units. None of these four are known structures, though 2_103 is expected to be highly chemically feasible ($\vartheta = 0.30$) as, to a lesser extent, is 2_55 ($\vartheta = 7.61$). By contrast, the ϑ values for 2_56 and 2_104 are 38.29 and 64.22, respectively.

We also define three more members of this family, 2_112, 2_102 and 2_80 (Figure 5f, h and j), which contain the mentioned [$3^2 5^6$] unit (Figure 5b), though with different building patterns. For example, in 2_112 the [$3^2 5^6$] units are linked via single oxygen

bridges (Figure 5h). As with all the structures belonging to this family, the two topologically distinct types of T-site are the 3-ring site (T1) and the "equatorial" site (T2). In 2_112, each unit is linked to twelve neighbours, with a T1 site of one unit always linked to a T2 site in a neighbouring unit (and *vice versa*). In this way, the larger cage (Figure 5i) is also formed and having 6-rings as its maximum aperture. A projection of the cubic unit cell is given in Figure 5g. In 2_102 (Figure 5j) the units are linked via double T1-T2 linkages, defining 4-rings (Figure 5k). This hexagonal structure is less dense than 2_112, with its pore system being accessible via 8-membered ring windows. In structure 2_80 (Figure 5l), the $[3^2 5^6]$ units are linked to one another by double T1-T1 and T2-T2 linkages (Figure 5m), defining large cages (Figure 5n) accessible through 8-ring channels running in all three directions. Both 2_112 and 2_102 are highly feasible, with ϑ = 4.66 and 6.08, respectively, as opposed to 2_80 which has ϑ = 87.12. For the latter structure, the topology imposes a degree of distortion on the $[3^2 5^6]$ polyhedra as can be seen in some of the concave T–O–T angles.

AWW family

There are nine structures which we describe as members of the "AWW family" since they share a small $[4^6 6^4]$ cage as the common building unit the (Figure 6a). Six of these structures, 2_88 (which has the actual AWW topology), 2_85, 2_59, 2_58, 2_100 and 2_63 are tetragonal, with columns of larger cages parallel to (001), having 8-ring windows as the maximum pore diameter in that direction. The archetypal example is the AWW $[4^8 6^8 8^2]$ cage (Figure 6b) which stacks through shared 8-rings (Figure 6e). Figure 6c shows the (001) projection of 2_85 which is typical of this series.

Depending on the linkage pattern of the $[4^6 6^4]$ building units along (001), different types of large cage are defined. In AWW, the $[4^6 6^4]$ units are connected "end-on", through shared 4-rings (Figure 6d). In 2_85, they alternate in orientation along the chain, with the shared 4-rings found on a mirror plane (Figure 6f). Two alternating types of larger cage are thus defined, $[4^8 6^{12} 8^2]$ and $[4^8 6^4 8^2]$ (also found in the known structures SAS and ATN respectively; Figure 6g). 2_59 has the $[4^6 6^4]$ units interspersed by D4R (Figure 6h), giving rise to larger $[4^{12} 6^4 8^6]$ (SAV) cages (Figure 6i). 2_58 also has two type of alternating cages, $[4^{12} 6^8 8^6]$ ("elongated alpha cage") and $[4^{12} 8^6]$ (Figure 6k), while 2_100 and 2_63 (Figure 6l-o) have only one type of 8-ring channel cage, denoted as $[4^4 5^8 6^4 8^2]$ and $[4^8 6^{12} 8^2]$, respectively. The first four structures (AWW, 2_58, 2_59 and 2_85) fall within the feasible range, with ϑ = 0.32 to 6.04, while 2_100 (ϑ = 22.42) and

2_63 (ϑ = 73.83) are less feasible. In the latter structure this is evidenced by the unfavourable T–O–T angles seen in Figure 6n.

There are also three cubic structures which contain the same building unit (2_109, 2_97 and 2_60), with 2_109 being by far the most feasible of the three (ϑ = 5.67). For these three structures, the $[4^6 6^4]$ units alternate with sodalite or beta cages in a chain along (100) (Figure 6p). Along (111) there are also chains of cages, with the repeat unit being three sodalite cages and one $[4^4 6^{14}]$ cage (Figure 6q). In 2_97, the chains of $[4^6 6^4]$ units alternate via a mirror plane (Figure 6r) and are extended in three directions of the structure, with $[4^4 5^4]$ units linked by 4-rings (Figure 6s) and producing the $[5^{12} 6^{20}]$ supercages (Figure 6t). The maximum aperture in this structure is again a 6-membered ring window. 2_60 has the $[4^6 6^4]$ units linked by D4R (Figure 6u) such that the chains intersect in three dimensions, thus defining large $[4^6 6^{24}]$ supercages (Figure 6v). 2_97 (ϑ = 16.99) falls within the extended range of oxide feasibility, whereas 2_60 (ϑ = 80.04) does not.

Supercage family

Eleven structures contain sodalite or LTA (alpha) cages linked by smaller prismatic units in such as way that it also generates much larger cages. All the structures have cubic or pseudo-cubic symmetry, an example of which can be seen in the (100) view of 2_45 (Figure 7a). Structure 2_74 has the framework of the mineral tschörtnerite (TSC) with both sodalite and alpha cages linked via D6R (Figure 7b), thus defining the large TSC cage (Figure 7c). The order in which the remaining structures are shown in Figure 7 is determined by their chemical feasibility factor, ϑ although it is convenient to discuss them in a slightly different order.

Structures 2_35 and 2_31 form a series together with the FAU structure, which is composed of sodalite cages linked tetrahedrally via D6R. Structure 2_35 is formed by replacing each single D6R in FAU by stacks of two D6R (Figure 7d). Similarly, 2_31 is generated by the addition of a third D6R to the stacks (Figure 7h). Consequently, the structures contain tetrahedral "super-faujasite" cages, accessible respectively through 18 and 24-membered rings (Figure 7e and i). As for FAU, the ideal topological symmetry of the two frameworks is *F*d-3m. However, on minimisation, 2_31 exhibits a slight preference for *R*-3m (i.e., there is a rhombohedral distortion). 2_35 and 2_31 are both feasible as oxide materials, with ϑ of 10.69 and 13.16, respectively. 2_45 and 2_36 can similarly be imagined as belonging to a series with RHO, a structure formed by alpha cages linked octahedrally via D8R. In fact, the RHO structure is body-centered, since

positioning the alpha cages on the lattice points of a primitive cubic lattice automatically defines a parallel network of alpha cages and D8R based on the body-centered lattice points. However, considering only the "primitive lattice" of cages, replacement of the D8R by stacks of two and three D8R gives structures 2_45 and 2_36 respectively (Figure 7f and v). Both have *P*m-3m symmetry and further contain cubic "super–LTA" cages with 12 and 16-membered ring apertures respectively (Figure 7g and w). Of the two, 2_45 is relatively feasible (ϑ = 12.91). 2_24 and 2_20 are related to the LTA structure, since they can be generated by linking sodalite cages and D4R. In 2_24, the D4R of the LTA structure are replaced by face-sharing stacks of two D4R (Figure 7j), and in 2_20 by stacks of three D4R (Figure 7p). They have the same supercages as 2_45 and 2_36 (Figure 7k and q), and similar ϑ of 13.28 and 16.11, respectively. 2_27 and 2_21 can also be considered part of a series with LTA, except in this case it is the alpha cages which are retained and the linkages between them expanded. While in LTA each alpha cage shares 12 D4R with its neighbours, in 2_27 an additional D4R is added to each link (Figure 7n), and 2_21 has stacks of three D4R (Figure 7r). The delineated "expanded sodalite" cages thus possess 9- and 12-membered rings, respectively (Figure 7o and s). The final pair, 2_39 and 2_32 form a series derived from KFI, containing alpha cages are connected via shared D6R which are replaced by stacks of two and three D6R in 2_39 and 2_32, respectively (Figure 7l and t). The supercages shown in Figure 7m and u may be denoted as $[4^{20}8^2 12^4]$ and $[4^{28}8^2 16^4]$, respectively, with both topologies ideally having *I*m-3m symmetry, as does KFI. Although in our modelling the 2_39 structure minimises into *P*1, it is the more feasible of the two with ϑ = 13.86.

SAS family

These structures are analogous to the AWW family as they contain stacks of large cages linked unidirectionally by 8-rings. Figure 8a shows the (001) projection of structure 2_54 which is typical of all four tetragonal structures belonging to this family and having *I*4/mmm space group symmetry (2_54, 2_57, 2_81(SAS) and 2_95). The basic building units may be thought of as smaller polyhedra arranged in parallel chains. In the case of 2_81, which has the SAS (STA-6) topology, the basic units are D6R hexagonal prisms, which form a chain by sharing 4-rings alternating in orientation (90° rotation) about *z* (Figure 8d), thus defining the classic $[4^8 6^{12} 8^2]$ SAS cages (Figure 8e). 2_95 is a highly feasible (ϑ = 0.93) structure in which $[4^4 5^4]$ units are linked into chains via 4-rings (Figure 8b), with the two types of alternating larger cages (Figure 8c) being

[$4^{12}8^6$] (also found in 2_58 and 2_62) and [$4^8 5^8 8^6$]. When compared to SAS, in 2_57 an additional D4R is interposed between the alternating D6R (Figure 8h), thus defining the larger cages (Figure 8i), which link to their neighbours through ten 8-membered ring apertures. 2_54 is built analogously, from chains of alternating D8R and D4R (Figure 8f) forming larger cages (Figure 8g) containing fourteen 8-membered rings and separated by D8R units. Aside from SAS and 2_95, both 2_54 and 2_57 are also quite feasible as zeolites (ϑ = 3.18 and 5.51, respectively).

[$4^2 5^8$] family

These structures have as a building unit the small [$4^2 5^8$] cage shown in Figure 9b. In four of the structures, these units are linked into chains through the 4-rings which cap the cages, in a very similar manner to the linking of the [$3^2 5^6$] units in that family. These structures are tetragonal with [$4^2 5^8$] chains running along (001), and have large cages accessible through 8-rings. The projection of 2_91 along (001) is typical of this family (Figure 9a). 2_91 (Figure 7a, c and d) is the most feasible of these structures (ϑ = 0.95), and has [$4^2 5^8$] cages linked through D4R, with a chain repeat motif of two cages and two D4R, plus a 45° twist being introduced at each cage. In 2_114, another highly feasible structure with ϑ = 2.17 (Figure 9e-f), the cages are directly linked through shared 4-rings, although each is still rotated by 45° about (001) with respect to its neighbours. 2_92 (with D4R spacers in the chain, Figure 9g-h) and 2_115 (direct 4-ring sharing, Figure 9i-j) are analogous structures to 2_91 and 2_114, respectively, but with only half the chain repeat distance, entailing considerable distortion of the [$4^2 5^8$] cages so that the 4-rings are translationally equivalent. Both structures are far less feasible, as is a fifth structure, 2_116 (Figure 9k-l), in which the [$4^2 5^8$] units are linked into chains via pairs of T–O–T linkages (Figure 9l). In the latter, the chains are interconnected so as to run in all three directions of the cubic lattice, and the structure also contains sodalite cages, each of which shares its 4-ring windows with [$4^2 5^8$] units.

AST family

Structure 2_101 (Figure 10a-c) is topologically identical to the known zeolite AST (AlPO-16) (Baerlocher & McCusker 2004; van Koningsveld 2004). The structure contains the characteristic [$4^6 6^{10}$] cages (Figure 10c) but may also be thought of in terms of D4R units connected through O–T–O bridges (Figure 10b). In this family we have also identified three other structures containing D4R, not directly linked through shared atoms. In 2_73 (Figure 10d-f), the D4R connect through single oxygen bridges and,

apart from containing sodalite cages, the structure also possesses the large tetrahedral cages shown in Figure 10f, which interconnect through 12-ring apertures. 2_61 (Figure 10g-i) is a tetragonal structure containing the cages shown in Figure 10i, which have oval-shaped 10-rings as their largest apertures. The D4R connect via a network of 6-rings and puckered 4-rings. Topologically, 2_13 (Figure 10j-l) is an elaboration of the AST structure in which those T-atoms which *do not* form part of D4R are replaced by $[3^4]$ tetrahedra of T-sites, a structural feature not found in aluminosilicate zeolites, although present, for instance, in the zeotypic sulphide RWY. Whilst bearing this proviso in mind, all three unknown structures can be considered chemically feasible, though not in "traditional" zeolite (or AlPO) compositions, having feasibility factors ϑ between 13.62 and 26.62. In addition to the $[3^4]$ unit, we note that the D4R is a structural feature shared with known germanate frameworks found in the range "extended" feasibility.

D8R family

This family is formed by four structures which contain the double 8-ring (D8R) as a structural unit. 2_47 (Figure 11a-c and f) has a cubic structure in which the building unit may be thought of as a D8R with four D4R attached to alternate 4-ring faces (Figure 11b-c). These units do not link directly to one another but are arranged so as to define the large $[4^{24}6^8 8^{18}]$ (TSC) cages shown in Figure 11f. The structure also contains stacks of LTA alpha cages, which alternate with smaller cages and are interconnected through 8-rings. 2_19 and 2_17 form part of a homologous series of structures, together with the uninodal structure 1_11 (Foster, et al. 2003), one of the nine simple uninodal tilings. The latter structure has a body-centered cubic framework based on chains of D8R and D4R which are linked in all three directions. 2_19 has the same structure, except that the D4R in 1_11 are replaced in 2_19 by pairs of face-sharing D4R (Figure 11d), and in 2_17 by groups of three D4R (Figure 11e). As a result, the large $[4^{60}8^6 18^8]$ and $[4^{84}8^6 24^8]$ cages shown in Figure 11g-h are defined. The more complex 2_34 structure (Figure 11i-k) also possesses the D8R/D4R units, but with the addition of $[4^6 6^4]$ AWW cages which link the units together through edge-sharing (Figure 11j), thus forming large cages having 12-rings as its maximum aperture (Figure 11k). Topologically, the tile which corresponds to this cage is the largest among this set of binodal frameworks, with 74 faces, 144 vertices and 216 edges. 2_34 shares the space group *I*m-3m with both 2_19 and 2_17. 2_47 is certainly thermodynamically feasible, with $\vartheta = 3.02$, while 2_17 and 2_19 have ϑ

= 13.96 and 13.39, respectively, despite having extremely low framework densities of 8.17 and 6.05 T/1000Å^3, respectively.

AFY family

Structure 2_50 is topologically identical to the known structural type AFY (AlPO-50). The secondary building unit of this family is a D4R, which in AFY form hexagonal layers (Figure 12a) and are "tilted" with respect to the 001 plane. These layers then repeat through simple translation along *c*, most clearly seen in (120) projection (Figure 12c) (Baerlocher & McCusker 2004; van Koningsveld 2004). If instead, the layers alternate in orientation by means of a mirror plane (i.e., ABA rather than AA) then framework 2_51 is formed (Figure 12b and d). The unit cell is roughly doubled in size along *c* and hence 2_51 has higher symmetry, $P6_3/mcm$ compared to $P\bar{3}1m$ for AFY. Both have low ϑ values: 5.03 and 5.18 for 2_50 and 2_51, respectively, making 2_51 virtually as feasible as AFY.

D6R family

This family comprises seven structures (2_6, 2_30, 2_53, 2_75, 2_76, 2_77 and 2_82) which have in common D6R hexagonal prisms as building units, although of these there are only two (2_76 and 2_75) for which D6R (i.e., 6-6) may be strictly defined as a secondary building unit. The structures are all cubic, space group *P*n-3m, with the exception of the two structures previously mentioned. The first five members of the group may be thought of in terms of chains running along (110) in which the D6R are linked by various combinations of rings. Each D6R is rotated by 60° with regard to its chain neighbours, with the chains in turn linking to form sheets along (100). This is clearly seen for 2_82 in Figure 13e, where the adjacent D6R are linked by units of two 4-rings and a 6-ring, with the latter bridging to an adjacent chain. A twisted 6-ring is thereby defined directly between the D6R. In the most feasible member of the family, 2_53 (ϑ = 5.11), the link unit includes D4R, giving rise to the characteristic motif shown in Figure 13b, where four D6R are connected to a single D4R. This structure also contains FAU supercages (Figure 13a) which are linked via the [$4^{18}8^6 12^2$] cages shown in Figure 13c. In these, the two puckered 12-rings are roughly parallel at an average distance of around 5.0 Å. In addition to the structural features already mentioned, 2_82 also possesses distorted [$4^{12}6^8 8^6$] alpha cages (Figure 13d) whose 8-rings are connected via the [$4^8 6^4 8^2$] cages (Figure 13f), which are topologically identical to the cages found in the ATN zeolite structures, although again the shape here is less regular with the

parallel 8-rings being elongated in orthogonal directions. 2_82 is another feasible structure with ϑ = 9.41. In 2_77, the D6R chains are linked by units of three 4-rings (Figure 13h), and the structure has FAU supercages, although much more distorted than in 2_53 (Figure 13g); in particular the 12-rings are puckered and exhibit a triangular distortion, with the [$4^{12}6^{6}12^{2}$] units linking supercages (Figure 13i) exhibiting -3 symmetry. In 2_30, the spiro-5 unit links the D6R into chains (Figure 13k) and a rather complex pore structure ensues, which is not trivial to describe, but some idea of its shape may be derived from Figure 13j: the largest pore apertures are elongated 12-rings and puckered 18-rings, an example of which is shown in Figure 13l. 2_77 and 2_30 are on the boundary of the extended range of feasibility with ϑ = 24.27 and 33.21, respectively, with 2_30 containing both 3 and 4-membered rings. 2_6 also contains 3-rings linked into [3^{4}] tetrahedra which connect the D6R as shown in Figure 13p. A complex pore structure analogous to that of 2_30 is thus generated (not shown) having puckered 24-rings (Figure 13q). Finally, structures 2_75 and 2_76 are the "odd ones out" of the family since it is not possible to describe them using the D6R chain model. 2_75 is very unusual as it contains both "regular" and flattened sodalite cages connected through 6-rings (Figure 13m, where the D6R are also illustrated). An oblate sodalite cage is shown in plan view in Figure 13n, whereas a large cavity, which links through puckered 12-membered ring pores, is shown in Figure 13o. 2_76 contains (differently) distorted beta cages (Figure 13r), as well as larger cages (Figure 13s) accessible through both approximately planar 6-rings and highly curved 8-rings. 2_75, 2_6 or 2_76 are not expected to be chemically feasible.

3- and 4-ring family

These eight structures are grouped together because they contain both 3 and 4-membered rings, although in other ways they are fairly different. Seven structures are cubic, and five have framework densities lower than 14 T/1000Å^{3}, illustrating the tendency of rare (i.e., the opposite of dense) structures to contain small rings. 2_99 (Figure 14a) can be described as a network of corner-sharing 3 and 4-rings, part of which is the unit illustrated in Figure 14b, a 3-ring linked to three 4-rings. Three types of cages can be found: the [$3^{8}8^{6}$] (truncated cube), shown in Figure 14c, [$4^{10}7^{4}8^{2}$] units (not shown) and [$4^{8}7^{12}$] (Figure 14d). This cubic structure is feasible, ϑ = 10.53, but contains unusual 7-membered rings, even despite the largest pores being formed by 8-rings. The somewhat similar 2_62 (Figure 14e), which has ϑ =10.97, also exhibits the truncated cube cage (Figure 14f), as well as D4R, [$4^{12}8^{6}$] cages similar to that found in

2_58 (Figure 6k) and the larger [$3^8 4^6 8^{12}$] cage shown in Figure 14g. 2_68 (Figure 14h) is tetragonal and has chains of 3-rings (Figure 14i) running along the (001) direction. It possesses cages (Figure 14j) linked through 10-membered ring pores, which form channels along (100) and (010). In a similar way to that observed for the remaining four structures in this family, 2_68 has a low framework density of 13.08 T/1000Å^3 and ϑ = 13.82. 2_70 and 2_93 have similar framework densities to that of 2_68 (13.42 and 13.98, respectively) and ϑ = 14.33 and 28.25, making these three structures interesting candidates as zeotypes. In 2_70 (Figure 14k), the 3-rings themselves form rings of eight via corner-sharing, which define chains of [$3^8 8^6$] truncated cubes (shown looking down the body diagonal in Figure 14l). The larger [$3^8 4^6 8^{12}$] cages shown in Figure 14m also describe a three-dimensional network. 2_93 possesses [$3^4 6^4$] cages, i.e., truncated tetrahedra (Figure 14o), which link through shared 3-rings to form a body-centred cubic structure, describing the [$4^6 6^{32}$] supercages shown in Figure 14p. Interestingly, despite its relatively low density, this structure does not contain rings larger than 6. 2_18, 2_28 and 2_5 have much lower framework densities (10.06, 11.69 and 7.28, respectively) than conventional zeolites, and correspondingly are much less feasible as zeotype materials. They are built from quite simple motifs: in 2_18 (Figure 14q-s) double 4-rings are linked in a three-dimensional network by spiro-5 units (i.e., two 3-rings sharing a T-atom), to form a body-centred cubic structure; the basic unit of structure 2_28 (Figure 14t-v) is a pair of edge-linked 3-rings (or bridged 4-ring), with two of these units being shown in Figure 14u, together with two linking 4-rings and the resulting large [$3^{12} 4^{12} 6^6 12^8$] cavity in Figure 14v; 2_5 is homologous with 2_18 but central T-site of the spiro-5 units is in this case replaced by a tetrahedron of T-sites. These three structures are very open, with 2_18 and 2_5 accessible through puckered 18- and 24-membered rings, respectively (see the "cages" illustrated in Figure 14s and y), whereas 2_28 has 12-ring channels along all {111} directions.

[$3^2 4^3$] D3R family

The common feature is a double 3-ring unit, i.e., a trigonal prism or a [$3^2 4^3$] unit, and we have assigned nine structures to this family. As in the previous family, many are of interest due to their low density, with the presence of small polyhedra being compensated by large supercages. While we believe that none is feasible in a traditional zeolite or AlPO composition, they may be well of interest in several areas of chemistry, for instance if it were possible to form the D3R unit as a precursor. All the structures are cubic and have at least m-3m symmetry. Structure 2_43 (Figure 15a) is the most

feasible (ϑ = 11.62) and has D3R units attached to [$3^4 6^4$] truncated tetrahedra to form tetrahedral units (Figure 15b). "Truncated cube" cages (see section 3.11) are present, as are the large [$4^{24}6^8 8^{18}$] cages shown in Figure 15c, and the largest accessible pore is an 8-ring. In 2_64 (Figure 15d), the D3R are also attached to truncated cube cages, but the structure additionally contains alpha and [$4^{24}6^8 8^{18}$] Tschörtnerite (TSC) cages (Figure 15e-f). Again, despite a very low framework density (10.14, compared to 9.71 for 2_43), the pore system is only accessible though 8-ring apertures. 2_23 (Figure 15g) has beta cages (Figure 15h) linked via D3R-4-ring-D3R bridging units. The large cavities (Figure 15i) have 16-membered rings in all three directions. 2_26 (Figure 15g) also has the same unit of two D3R linked though a 4-ring (as do 2_25 and 2_22), with alpha cages present, but the main pore system is defined by the tetrahedral [$3^{12}6^4 12^4$] and the larger [$4^{24}8^6 12^8$] cages (Figure 15k-l), which are linked through 12-ring pores. The latter cavity has the same topology as that found in structure 1_11.(Foster, et al. 2003) Structure 2_25 (Figure 15m) has a pore system connected through 12-ring apertures and contains not only FAU supercages and LTA alpha cages, but also the large [$4^{24}8^6 12^8$] cages (Figure 15n) which are found in the RWY structure, and correspond in a topological sense to truncated sodalite cages (each T-site of the sodalite cage is replaced by a 3-ring). 2_41 (Figure 15o) has similarities to 2_43 as the D3R form an alternating network with truncated tetrahedra (as in Figure 15b). In this case, the units form a continuous network, thereby defining very large [$4^{36}6^{24}8^6 12^8$] cages shown in Figure 15p, which is reflected in its low framework density (F_D = 8.99 T/1000Å^3). 2_22 (Figure 15q) is also of very low density (F_D = 9.70 T/1000Å^3), and has the D3R connected so as to define D8R (Figure 15r). The already discussed large [$4^{24}8^6 12^8$] and RWY cages (Figure 15s-t) are present, and linked through 12-rings. Finally 2_4 and 2_8 (Figure 15u and x) are among the least dense of all the binodal simple tile structures, with F_D of 5.39 and 6.48 T/1000Å^3 respectively. The basic building unit of 2_8 is two D3R stacked with an intervening D4R (Figure 15v). In 2_4 the intermediate unit is absent, and D3R units join directly through a shared 4-ring (Figure 15y). In both cases, very open cavity systems are constructed by connection of these units, as seen in Figure 12w-z.

3-ring family

This family of eight structures is characterised by the presence of 3-rings. Five structures contain pairs, or longer chains, of 3-rings which share one T-atom, and therefore contain the spiro-5 unit (Baerlocher, et al. 2001). Two of the structures also contain 4-rings, but have more affinity with the others in this family, rather than with

the more symmetric structures in previous families. As expected, several of the structures are of low density, but none would be expected to be realisable as a "conventional" zeolite, 2_71 being the most feasible with $\vartheta = 17.07$. In 2_71 (Figure 16a), 3-rings themselves form rings of six (Figure 16b), with the structure also containing elongated cages having 8-rings as their largest pore, these cages being of somewhat irregular appearance (Figure 16c). The basic unit of 2_69 is a pair of edge-sharing 3-rings (or bridged 4-ring), which link as shown in Figure 16e. These larger units then connect to define the hexagonal channel system (Figure 16d), of which a puckered 12-ring forms the characteristic pore. 2_65 (Figure 16f) also contains loops of six 3-rings (Figure 13g), virtually identical in structure to those present in 2_71. However, the structure is much more open ($F_D = 12.28$, compared to 17.38 for 2_71), containing a three-dimensional network of 10 and 12-ring pores (the latter shown in Figure 16h), defined by the 3-ring network. 2_44 (Figure 16i) is another very open structure ($F_D = 10.36$), with a three-dimensional network of corner-sharing 3-rings defining the small $[3^4 6^4]$ cages shown in Figure 16j, as well as large cavities linked through 12-rings. 2_12 has unusual chains built up from pairs of edge-sharing 3-rings (Figure 16l). This structure is tetragonal and has large cross-linked channels extending in two dimensions, delineated by puckered 14-membered rings. 2_29 (Figure 16m) is an unusually complex cubic structure, with 3 and 4-rings linked together as shown in Figure 16n: pairs of 3-rings are formed which edge-share (there are no spiro-5), and these pairs are further connected by distorted 4-rings. Both 9-rings and 12-rings are thus formed (Figure 16o-p), with former forming channels along the (111) direction. Uniquely for this family, in 2_105 (Figure 16q), the 3-rings do not directly link into chains or pairs through the sharing of T-atoms, but rather connect through O bridges to define 5-rings (Figure 16r). This ideally trigonal structure (but which optimises in space group *P*1) has large-pore type channels defined by puckered 12-rings. Finally, 2_9 (Figure 16s) has "H-shaped" building units in which 4-rings share edges with pairs of 3-rings (Figure 16t). On a larger scale, the structure has unidirectional channels defined by puckered 18-membered rings, similar to those present in 2_30 (Figure 13l).

$[3^4]$ family

The common feature of this family is a $[3^4]$ unit, sometimes known as the "supertetrahedron" or tetrahedron of tetrahedra. As already mentioned, this unit is unknown in zeolitic oxide materials, but is present in some sulphide materials, including the zeotypic RWY structure and the compound $Na_2Si_2S_5$. 2_16 (Figure 17a-b),

one of the few structures here containing 7-rings, is characterised by its [$3^8 4^2 7^8 8^4$] cage shown in Figure 17b. Each of the eight 3-rings forms part of a [3^4] unit, shared with three other cages. This structure is the most "feasible" of this family, with $\vartheta = 36.19$. An alternative description of the structure lies in the fact that it can be derived from the clathrasil-like 2_117 (see the "orphan" section below) by replacement of one of the unique types of T-site by a tetrahedron of T-sites. In a similar way, 2_14 (Figure 17c-d) has only one type of "larger" cage, [$3^8 4^2 6^4 8^8$], and the whole structure can be thought of in terms of the sodalite framework, but with one third of the T-sites replaced by [3^4] supertetrahedra. 2_15 (Figure 17e-f) is also related to the sodalite structure, though now with half of the original T-sites replaced by the [3^4] units, creating [$3^{12} 6^6 9^8$] cages. 2_10 (Figure 17g-i) can be derived from the RHO zeolite structure by replacement of all T-sites by [3^4] tetrahedra. As a result it possesses very large cages linked via double 16-membered rings (Figure 17i). Finally, structure 2_7, being the least dense of this family ($F_D = 8.60$), has [$3^4 6^4$] units ("truncated tetrahedra") linked via chains of 4-rings and [3^4] units. This very open cubic structure has 16-MR pores in all three dimensions.

Orphan structures

Some structures cannot be categorised in our "family" system.

2_117 (Figure 18a-b) is a highly feasible ($\vartheta = 1.22$) clathrasil-type structure containing 4, 5 and 6-rings. It has only one type of cage, [$4^2 5^8 6^4$], which is shown in Figure 18b.

2_113 (Figure 18c-d) also has only one type of cage, made up of 4, 5 and 6-rings. In this case, however, the [$4^4 5^4 6^4$] cage is chiral, with the structures being built up from alternating layers of the two enantiomeric forms of the cage. Furthermore, the structure is also feasible as a zeolite with $\vartheta = 5.32$.

2_96, another feasible zeolite structure ($\vartheta = 5.45$), is unusual as it contains small [$4^5 5^2 6^2$] cage units (Figure 18e) interconnected through shared 4-rings to form a three-dimensional network (Figure 18f), thereby defining the [$5^{12} 6^{20}$] cage shown in Figure 18g (which also appears in structure 2_97).

2_67 (Figure 18h-j) is built up from twisted sheets of 4-membered rings, which include "squares" of four 4-rings (Figure 18i). The large cages (Figure 18j), reminiscent of those of faujasite, define a three-dimensional network of 12-membered ring pores. For this structure $\vartheta = 10.27$.

2_37 (Figure 18k-m). The basic building unit is the D4R, which links via 4-rings to create double 12-membered rings (Figure 18l), which are in turn linked into large

[$4^{36}8^{4}12^{8}$] supercages (Figure 18m). These supercages have tetrahedral symmetry, with four puckered 12-rings and four 12-rings which are almost planar. Overall, this cubic structure is quite open with F_D = 12.58 T/1000Å^3, but is of intermediate feasibility (ϑ = 18.50).

2_48 (Figure 18n-p) also contains D4R units, which, together with elongated D8R, form a three-dimensional network (Figure 18o) having large [$4^{24}8^{6}9^{8}$] cages as depicted in Figure 18p; a 9-ring thus defines the largest pore present in the structure, which again is feasible (ϑ = 19.09), though we predict not as a "conventional" zeolite.

2_52 (Figure 18q-s). Another cubic structure containing D4R, which in this case form "butterfly-like" units (Figure 18q) with four 4-rings. [$4^{24}6^{4}12^{4}$] FAU supercages (Figure 18s) are also present, and so the structure has a network of 12-ring pores. ϑ = 20.93.

2_79 (Figure 18t-v) possesses a three-dimensional network of distorted sodalite cages, linked as shown in Figure 18u. The structure also contains D6R and D8R, the latter separating LTA cages as depicted in Figure 18v. For this structure ϑ = 23.48, which renders the remaining members of this family increasingly less probable candidates for zeolite synthesis.

2_46 (Figure 18w-y) is similar to 2_67 as it contains no small cages or prismatic units, but can rather be described in terms of a continuous sheet of 4- and 6-rings, a section of which is shown in Figure 18x. Topologically, the sheet is equivalent to the Schwarz D surface (Gandy, et al. 1999), and as a consequence the pore system is divided into two identical but non-intersecting volumes, with the centres of the large cages forming two interpenetrating diamond lattices. These cages, shown in Figure 18y, are connected through 12-ring apertures.

2_94 (Figure 18z and aa). This structure contains [$3^{4}6^{4}$] truncated tetrahedra, distorted sodalite cages, and larger cages with 3- and 6-rings, seen in Figure 18aa. The ideal symmetry of the structure is *F*d-3m. However, in silica form, it appears highly strained in this symmetry, preferring to minimise in space group *C*121, hence giving rise to the somewhat distorted appearance.

Like 2_94, 2_98 (Figure 18bb-cc) is a dense structure (F_D = 20.69 T/1000Å^3). Based on edge-sharing chains of 4-rings, the structure has as its largest pore the twisted 8-ring shown in Figure 18cc.

2_111 (Figure 18dd-ff) is both highly dense (22.87 T/1000Å^3) and unfeasible as a zeolite (ϑ = 43.36). However, it is remarkable as it contains 3-, 5-, 6- and 7-rings, from

which a 7-ring is illustrated in Figure 18ff. A characteristic feature of 2_111 is the "cup"unit shown in Figure 18ee, composed of a 3-ring and three 5-rings.

Finally, 2_42 (Figure 18gg-ii) has triple 8-membered rings (Figure 18hh), as well as $[4^4 5^4]$ units. Although of relatively high density (17.94), it still has large $[4^{24}5^{24}8^6 12^8]$ cavities (Figure 15ii), linked into a three-dimensional network through puckered 12-membererd rings.

Conclusions

We have evaluated and characterised 109 hypothetical zeolite structures, of which 98 do not correspond to known zeotype frameworks. Among these are many very interesting candidates for zeolite synthesis. Some of the most feasible as conventional aluminosilicates or AlPOs are those in the ABC-6 family, composed principally of 4- and 6-rings, though from the point of view of porosity, the more likely structures will be at best small-pore zeolites, having no aperture larger than the 8-ring. Other promising candidates come from structures which similarly have features in common with known zeolites, such as those in the AWW and SAS families (Figures 3 and 5), where cages stack through shared 8-rings. Again, 4 and 6-rings predominate, with the 8-ring being the limiting aperture in all cases, as it is for the more feasible structures in the $[4^2 5^6]$ family (Figure 6). At the other end of the scale, many very open structures also exist. These illustrate well the principle originally due to Meier (Brunner & Meier 1989) that less dense structures invariably require a greater proportion of "small" (3- or 4-) rings as compensation. Here, we can extend this to state that larger cavities also require the presence of much smaller cages. Hence we find large-pore structures containing $[3^4]$ units (Figure 14), double-3-rings (Figure 12) and double 4-rings (e.g., Figures 7 and 8) 3-rings as well as pairs and chains of 3- and 4-rings. In terms of aluminosilicate (and aluminophosphate) zeolites, these structural units, particularly those containing 3-rings, are by-and-large disfavoured due to the strain imposed on the TO_4 tetrahedra. In fact it is apparent that feasibility decreases markedly as more 3-rings are connected together with, for example, structures containing $[3^4]$ units having higher values than those containing only spiro-5 units. The most viable 3-ring structures are those in which the 3-rings are isolated from one another. The best example is 2_103 which contains the $[3^2 5^6]$ unit (Figure 5b), reminiscent of the $[3^1 4^3 5^3]$ units in the MEI structure. 2_103 is the most feasible large-pore zeolite among our 109 structures. Similarly, although 4-rings are found in the most feasible structures, agglomerations of

these units, obtained for example by stacking prismatic units such as D4R and D6R, result in decreasing likelihood (though individual D4R and D6R are tolerated, unlike D3R).

Having discounted many of the more open structures as potential zeolites on account of the presence of these small units, we do not exclude the possibility that these topologies could be possible in other chemical compositions where the local coordination environments are less constrained. Indeed, if we could construct units such as the D3R or the supertetrahedron as precursor species, many open framework architectures could be synthesized.

Acknowledgements. We are grateful to the EPSRC (U.K.) and to the Leverhulme Trust for support, and to the Portuguese Foundation for Science and Technology (FCT) for the Ph.D. scholarship No. SFRH/BD/3024/2000 to F.A.A.P.

Figure Captions

Figure 1. Framework energy, E_F (kJ/mol), with respect to α-quartz, versus framework density (Si atoms per 1000 $Å^3$) for **(a)** and **(b)** all known zeolitic structure types; **(c)** and **(d)** hypothetical binodal zeolitic structures.

Figure 2. Accessible volume ($Å^3$ per Si atom) versus framework density for **(a)** all known zeolitic structure types; **(b)** hypothetical binodal zeolitic structures; **(c)** structures with accessible volumes below 40 $Å^3$ per Si atom.

Figure 3. Framework energy with respect to α-quartz versus accessible volume ($Å^3$ per Si atom) for **(a)** all known zeolitic structure types; **(b)** hypothetical binodal zeolitic structures. Hypothetical structures of particular chemical interest are identified in the inset.

Figure 4. Molecular graphic illustrations of structures from the ABC-6 family.

Figure 5. Molecular graphic illustrations of structures from the $[3^25^6]$ family.

Figure 6. Molecular graphic illustrations of structures from the AWW family.

Figure 7. Molecular graphic illustrations of structures from the Supercage family.

Figure 8. Molecular graphic illustrations of structures from the SAS family.

Figure 9. Molecular graphic illustrations of structures from the $[4^25^8]$ family.

Figure 10. Molecular graphic illustrations of structures from the AST family.

Figure 11. Molecular graphic illustrations of structures from the D8R family.

Figure 12. Molecular graphic illustrations of structures from the AFY family.

Figure 13. Molecular graphic illustrations of structures from the D6R family.

Figure 14. Molecular graphic illustrations of structures from the 3 and 4-ring family.

Figure 15. Molecular graphic illustrations of structures from the D3R family.

Figure 16. Molecular graphic illustrations of structures from the 3-ring family.

Figure 17. Molecular graphic illustrations of structures from the [3^4] family.

Figure 18. Molecular graphic illustrations of the Orphan Structures.

References

Akporiaye, D. E. & Price, G. D. 1989 Systematic enumeration of zeolite frameworks. *Zeolites* 9, 23-32.

Alberti, A. 1979 Possible 4-connected frameworks with 4-4-1 unit found in heulandite, stilbite, brewsterite, and scapolite. *Am. Mineral.* 64, 1188-1198.

Baerlocher, C. & McCusker, L. B. 2004 http://www.iza-structure.org/databases.

Baerlocher, C., Meier, W. M. & Olson, D. H. 2001 *Atlas of Zeolite Structure Types (updates on http://www.iza-structure.org/)*. London: Elsevier.

Barrer, R. M. & Villiger, H. 1969 The crystal structure of the synthetic zeolite L. *Z. Kristallogr.* 128, 352-370.

Bialek, R. 1995 KRIBER, version 1.1. *Institut für Kristallographie und Petrographie, ETH: Zürich, Switzerland*

Boisen, M. B., Gibbs, G. V., O'Keeffe, M. & Bartelmehs, K. L. 1999 A generation of framework structures for the tectosilicates using a molecular-based potential energy function and simulated annealing strategies. *Microporous Mesoporous Mat.* 29, 219-266.

Brunner, G. O. & Meier, W. M. 1989 Framework density distribution of zeolite-type tetrahedral nets. *Nature* 337, 146-147.

Cerius^2 1999 *v. 4.0, Molecular Simulations Inc., San Diego*

Connolly, M. L. 1985 Computation of molecular volume. *J. Am. Chem. Soc.* 107, 1118-1124.

Delgado Friedrichs, O. 2001 Recognition of flat orbifolds and the classification of tilings in R-3. *Discret. Comput. Geom.* 26, 549-571.

Delgado Friedrichs, O., Dress, A. W. M., Huson, D. H., Klinowski, J. & Mackay, A. L. 1999 Systematic enumeration of crystalline networks. *Nature* 400, 644-647.

Dress, A. W. M., Huson, D. H. & Molnár, E. 1993 The classification of face-transitive periodic 3-dimensional tilings. *Acta Cryst.* A49, 806-817.

Foster, M. D. & Treacy, M. M. J. 2004 Hypothetical Zeolites: Enumeration Research. *Hypothetical Zeolites: Enumeration Research, http://www.hypotheticalzeolites.net/*

Foster, M. D., Bell, R. G. & Klinowski, J. 2001 Characterisation of hypothetical zeolite frameworks. *Stud. Surf. Sci. Catal.* 136, 266.

Foster, M. D., Delgado Friedrichs, O., Bell, R. G., Almeida Paz, F. A. & Klinowski, J. 2003 Structural evaluation of systematically enumerated hypothetical uninodal zeolites. *Angew. Chem. Int. Edit.* 42, 3896-3899.

Foster, M. D., Friedrichs, O. D., Bell, R. G., Almeida Paz, F. A. & Klinowski, J. 2004a Chemical evaluation of hypothetical uninodal zeolites. *J. Am. Chem. Soc.* 126, 9769-9775.

Foster, M. D., Simperler, A., Bell, R. G., Delgado Friedrichs, O., Almeida Paz, F. A. & Klinowski, J. 2004b Chemically feasible hypothetical crystalline networks. *Nature Materials* 3, 234-238.

Gandy, P. J. F., Cvijovic´, D., Mackay, A. L. & Klinowski, J. 1999 Exact computation of the triply periodic D ('diamond') minimal surface. *Chem. Phys. Lett.* 314, 543-551.

GDIS 2004 *version 0.84, SourceForge*

Henson, N. J., Cheetham, A. K. & Gale, J. D. 1994 Theoretical calculations on silica frameworks and their correlation with experiment. *Chem. Mater.* 6, 1647-1650.

Hu, Y. T., Navrotsky, A., Chen, C. Y. & Davis, M. E. 1995 Thermochemical study of the relative stability of dense and microporous aluminophosphate frameworks. *Chem. Mat.* 7, 1816-1823.

Klinowski, J. 1998 Hypothetical molecular sieve frameworks. *Current Opinion in Solid State & Materials Science* 3, 79-85.

Liebau, F., Gies, H., Gunawardane, R. P. & Marler, B. 1986 Classification of tectosilicates and systematic nomenclature of clathrate type tectosilicates: a proposal. *Zeolites* 6, 373-377.

Meier, W. M. & Villiger, H. 1969 The crystal structure of the synthetic zeolite L. *Z. Kristallogr.* 128, 352-370.

Mellot-Draznieks, C., Newsam, J. M., Gorman, A. M., Freeman, C. M. & Férey, G. 2000 De novo prediction of inorganic structures developed through automated assembly of secondary building units (AASBU method). *Angew. Chem. Int. Edit.* 39, 2270-2275.

Mellot-Draznieks, C., Girard, S., Férey, G., Schön, J. C., Cancarevic, Z. & Jansen, M. 2002 Computational design and prediction of interesting not-yet-synthesized structures of inorganic materials by using building unit concepts. *Chem. Eur. J.* 8, 4103-4113.

Moloy, E. C., Davila, L. P., Shackelford, J. F. & Navrotsky, A. 2002 High-silica zeolites: a relationship between energetics and internal surface areas. *Microporous Mesoporous Mat.* 54, 1-13.

Navrotsky, A., Petrovic, I., Hu, Y. T., Chen, C.-Y. & Davis, M. E. 1995 Little energetic limitation to microporous and mesoporous materials. *Microporous Mater.* 4, 95-98.

O'Keeffe, M. & Hyde, S. T. 1996a The asymptotic behavior of coordination sequences for the 4-connected nets of zeolites and related structures. *Z. Kristallogr.* 211, 73-78.

O'Keeffe, M. & Hyde, B. G. 1996b *Crystal Structures I: Patterns and Symmetry*. Washington, D.C.: Mineralogical Association of America Monograph.

Petrovic, I., Navrotsky, A., Davis, M. E. & Zones, S. I. 1993 Thermochemical study of the stability of frameworks in high-silica zeolites. *Chem. Mater.* 5, 1805-1813.

Piccione, P. M., Yang, S. Y., Navrotsky, A. & Davis, M. E. 2002 Thermodynamics of pure-silica molecular sieve synthesis. *J. Phys. Chem.* B106, 3629-3638.

Piccione, P. M., Woodfield, B. F., Boerio-Goates, J., Navrotsky, A. & Davis, M. E. 2001 Entropy of pure-silica molecular sieves. *J. Phys. Chem.* B105, 6025-6030.

Piccione, P. M., Laberty, C., Yang, S. Y., Camblor, M. A., Navrotsky, A. & Davis, M. E. 2000 Thermochemistry of pure-silica zeolites. *J. Phys. Chem. B* 104, 10001-10011.

POV-Ray 2004 *version 3.6, Persistence of Vision Raytracer Pty. Ltd.*

Sastre, G. & Gale, J. D. 2001 ZeoTsites: a code for topological and crystallographic tetrahedral sites analysis in zeolites and zeotypes. *Microporous Mesoporous Mat.* 43, 27-40.

Sato, M. 1984 Framework topology and systematic derivation of zeolite structures, *Proceedings of the 6th International Zeolite Conference, Reno, U.S.A., 10-15 July 1983*, (ed. D. H. Olson & A. Bisio), Guildford, U.K.: Butterworths.

Sato, M. 1987 Framework topology of tectosilicates and its characterization in terms of coordination degree sequence. *J. Phys. Chem.* 91, 4675-4681.

Sherman, J. D. & Bennett, J. M. 1973 Framework structures related to the zeolite mordenite, *Molecular Sieves*, (ed. W. M. Meier & J. B. Uytterhoeven), Washington, DC: American Chemical Society.

Simperler, A., Foster, M. D., Bell, R. G. & Klinowski, J. 2004 Hypothetical uninodal zeolite structures: comparison of $AlPO_4$ and SiO_2 compositions using computer simulation. *J. Phys. Chem.* B108, 869-879.

Smith, J. V. 1988 Topochemistry of zeolites and related materials. 1. Topology and geometry. *Chem. Rev.* 88, 149-182.

Smith, J. V. 1993 Topology of nets and stereochemistry of molecular sieves. *ACS Abstracts* 205, 157-IEC.

Treacy, M. M. J., Randall, K. H., Rao, S., Perry, J. A. & Chadi, D. J. 1997 Enumeration of periodic tetrahedral frameworks. *Z. Kristallogr.* 212, 768-791.

van Koningsveld, H. 2004 Schemes for Building Zeolite Structure Models. *Schemes for Building Zeolite Structure Models, in Database of Zeolite Structures,* http://topaz.ethz.ch/IZA-SC/ModelBuilding.htm

Wells, A. F. 1977 *Three-Dimensional Nets and Polyhedra*. New York: Wiley.

Wells, A. F. 1979 *Further Studies of Three-Dimensional Nets, American Crystallographic Association Monograph No. 8*. Pittsburgh: Polycrystal Book Service.

Wells, A. F. 1984 *Structural Inorganic Chemistry*. Oxford: Oxford University Press.

Table 1. Chemical feasibility factor, relative lattice energy, framework density and coordination sequences for 109 hypothetical binodal zeolites, optimised as purely siliceous structures. Structures are listed in order of increasing value of ϑ.

Structure	ϑ	ΔE_{quartz} [kJ/mol]	F_D [T-sites/1000 Å^3]	Coordination sequence									
2_87	0.10	15.91	16.86	4	9	17	30	49	72	96	121	150	187
				4	10	20	33	49	69	94	125	160	197
2_89 (ERI)	0.12	16.39	16.51	4	9	17	30	50	75	98	118	144	185
				4	10	20	32	46	64	90	126	164	196
2_84 (EAB)	0.12	16.41	16.49	4	9	17	30	49	71	92	115	147	190
				4	10	20	32	46	66	94	128	162	192
2_90 (SAT)	0.18	15.72	16.91	4	9	17	30	50	75	100	126	157	194
				4	10	20	33	50	71	95	124	158	197
2_103	0.30	16.80	16.04	4	10	17	30	52	70	107	128	166	208
				4	11	20	33	51	73	103	136	169	207
2_88 (AWW)	0.32	15.03	17.25	4	9	17	30	50	74	97	123	158	198
				4	10	20	33	50	72	98	128	162	200
2_86	0.37	15.54	16.85	4	9	17	30	49	72	96	121	150	186
				4	10	20	33	49	68	92	122	155	191
2_83 (LEV)	0.42	16.00	16.48	4	9	17	30	49	71	92	114	143	183
				4	10	20	32	46	64	90	124	156	184
2_85	0.69	16.03	17.57	4	9	17	30	49	71	95	125	161	201
				4	10	20	33	50	73	100	131	168	208
2_107 (LOS)	0.91	13.86	17.47	4	10	20	34	52	74	102	136	172	210
				4	10	20	34	54	78	104	134	168	210
2_74 (TSC)	0.94	19.47	13.55	4	9	16	25	37	53	74	99	125	151
				4	9	17	28	41	56	73	93	117	146
2_110	0.94	13.82	17.47	4	9	17	30	50	74	97	123	158	198
				4	10	20	33	50	72	98	128	162	200
2_106	0.97	13.79	17.46	4	10	20	34	52	74	100	130	166	208
				4	10	20	34	53	76	103	135	170	209
2_95	0.93	17.49	16.80	4	9	18	32	52	75	99	133	171	207
				4	10	19	32	52	76	103	136	172	213
2_108	0.97	13.77	17.47	4	10	20	34	53	76	102	132	167	208
				4	10	20	34	53	76	103	135	170	208
2_81 (SAS)	0.98	15.88	16.00	4	9	17	30	48	68	87	109	142	184
				4	10	19	30	45	65	90	118	145	175

2_91	0.95	17.12	17.07	4	9	17	31	54	82	108	137	176	223
				4	11	22	35	55	81	107	143	184	222
2_78 (AFX)	1.00	16.41	15.61	4	9	17	29	45	64	85	110	141	178
				4	9	17	29	45	65	89	116	144	175
2_101 (AST)	0.99	18.14	16.41	4	9	19	34	48	66	96	127	151	183
				4	12	18	28	52	78	88	112	162	204
2_117	1.22	11.58	18.74	4	11	24	41	64	93	127	163	205	255
				4	12	22	44	64	94	124	164	206	252
2_114	2.17	11.15	18.09	4	11	21	36	64	93	120	156	202	255
				4	11	23	40	62	88	123	162	202	249
2_47	3.02	24.55	14.00	4	9	17	28	41	56	74	97	125	158
				4	8	14	24	37	54	75	97	121	148
2_54	3.18	24.09	14.47	4	8	14	25	40	57	76	96	119	150
				4	9	17	27	38	54	76	101	128	154
2_112	4.66	20.19	18.66	4	10	22	40	60	95	121	165	212	258
				4	12	21	41	67	90	128	168	211	263
2_50 (AFY)	5.03	27.27	14.12	4	8	14	25	39	53	71	96	124	152
				4	9	16	23	34	57	82	98	115	141
2_53	5.11	26.05	15.05	4	7	12	24	39	60	79	110	168	250
				4	10	19	27	39	62	92	137	202	275
2_51	5.18	27.49	14.12	4	8	14	25	39	53	72	100	130	157
				4	9	16	23	34	57	82	98	118	153
2_59	5.25	23.49	16.96	4	9	18	32	52	75	99	133	171	207
				4	10	19	32	52	76	103	136	172	213
2_113	5.32	18.94	20.19	4	10	23	38	60	86	118	154	195	244
				4	11	21	39	61	86	118	154	195	243
2_96	5.45	24.88	16.21	4	9	18	32	52	75	105	144	181	217
				4	11	21	35	54	80	113	145	182	228
2_57	5.51	25.91	15.54	4	8	14	26	44	63	80	97	122	164
				4	10	19	28	39	57	82	112	139	159
2_109	5.67	21.61	18.68	4	10	20	34	53	76	102	133	170	212
				4	10	20	34	53	77	106	139	174	212
2_58	6.04	24.64	16.95	4	8	14	26	45	67	89	115	149	188
				4	10	20	32	47	68	93	122	157	196
2_102	6.08	26.50	15.70	4	9	19	34	48	73	98	125	167	197
				4	11	18	31	54	72	96	128	160	204
2_55	7.61	29.43	15.20	4	8	14	26	44	62	91	121	144	181
				4	11	19	29	47	67	91	121	153	188
2_82	9.41	27.74	18.17	4	9	17	30	48	69	92	119	153	192
				4	10	20	32	46	66	94	126	158	194
2_67	10.27	33.41	15.11	4	8	16	28	42	60	84	108	136	170
				4	9	16	27	43	62	83	109	139	171

2_99	10.53	30.91	17.10	4	9	18	34	55	76	103	144	187	229
				4	9	20	34	54	81	110	144	185	229
2_35	10.69	41.65	9.82	4	8	13	20	28	36	46	62	83	104
				4	9	15	21	28	37	49	65	85	108
2_62	10.97	33.96	15.43	4	8	14	27	48	70	91	116	146	185
				4	9	19	32	45	67	92	124	165	209
2_43	11.62	41.22	11.05	4	8	14	21	34	53	71	90	108	133
				4	8	16	27	35	48	66	83	113	146
2_64	12.15	41.09	11.67	4	8	15	25	37	52	71	95	120	148
				4	8	16	27	37	53	71	89	116	144
2_45	12.91	40.22	13.03	4	8	14	23	34	49	67	87	111	139
				4	9	16	25	37	52	70	91	114	140
2_31	13.16	48.71	7.40	4	8	12	17	24	31	36	42	54	72
				4	9	15	20	24	29	37	48	60	73
2_24	13.28	43.16	11.36	4	7	12	22	32	41	56	80	106	125
				4	9	15	22	32	46	63	81	100	122
2_19	13.39	47.93	8.17	4	7	10	16	22	26	34	48	63	76
				4	8	12	16	21	28	37	49	64	80
2_73	13.62	38.71	14.78	4	9	15	21	37	59	104	138	182	199
				4	11	20	36	52	77	121	155	192	236
2_68	13.82	41.46	13.08	4	8	17	28	45	66	88	114	141	182
				4	9	16	28	48	66	84	115	150	178
2_39	13.86	39.83	14.25	4	8	13	22	36	53	72	94	122	156
				4	9	16	25	38	56	78	103	129	157
2_17	13.96	51.80	6.05	4	7	9	13	19	23	25	30	41	55
				4	8	12	15	17	21	28	36	44	53
2_70	14.33	41.70	13.42	4	8	17	32	46	71	95	129	166	199
				4	9	18	32	50	70	95	128	166	212
2_40	14.97	40.32	15.02	4	8	13	22	37	56	76	98	126	158
				4	9	16	26	41	60	80	101	126	158
2_27	15.42	42.76	13.78	4	7	12	24	38	50	68	94	122	153
				4	9	16	26	40	57	78	103	130	159
2_23	15.97	51.69	8.14	4	7	12	20	26	32	44	68	90	108
				4	8	13	17	24	34	49	67	82	101
2_20	16.11	50.76	8.93	4	7	10	17	27	35	41	52	73	100
				4	9	15	20	25	33	47	66	84	98
2_97	16.99	40.46	16.94	4	9	18	32	52	76	106	147	188	229
				4	11	21	35	55	81	117	152	188	238
2_71	17.07	39.95	17.38	4	8	19	39	58	83	118	160	193	232
				4	10	21	38	58	91	117	158	195	244
2_26	17.51	50.60	10.44	4	7	12	22	34	46	58	76	107	139
				4	8	14	21	32	48	65	86	111	138

2_25	17.56	50.63	10.47	4	7	12	22	33	44	58	80	104	125
				4	8	14	21	32	48	65	85	106	132
2_37	18.50	48.93	12.58	4	8	12	17	24	31	36	42	54	72
				4	9	15	20	24	29	37	48	60	73
2_21	18.85	49.90	12.26	4	7	10	18	32	47	59	71	91	121
				4	9	16	24	34	48	66	89	117	149
2_32	19.04	49.98	12.40	4	8	12	18	29	44	60	77	98	125
				4	9	16	24	33	45	62	85	113	143
2_48	19.09	45.87	15.29	4	8	14	25	38	50	70	100	125	147
				4	9	16	24	36	56	76	92	120	159
2_41	19.44	55.48	8.99	4	8	14	19	26	40	52	70	88	100
				4	8	14	20	29	42	52	68	89	109
2_69	20.57	49.50	14.25	4	8	17	29	46	68	91	117	154	184
				4	9	17	28	49	69	92	119	151	184
2_65	20.64	52.45	12.28	4	8	15	28	47	66	86	118	155	181
				4	8	16	26	48	66	88	120	142	200
2_33	20.83	49.10	14.80	4	8	12	18	30	49	71	92	114	143
				4	9	16	25	38	56	77	99	121	147
2_52	20.93	48.51	15.30	4	7	10	16	25	34	43	58	75	90
				4	7	11	16	24	35	46	59	75	93
2_100	22.42	45.32	19.00	4	9	18	34	58	86	113	146	194	248
				4	11	22	38	61	88	120	157	199	246
2_79	23.48	45.37	20.03	4	9	17	29	46	69	98	133	174	221
				4	10	21	37	58	84	114	148	186	229
2_77	24.27	47.94	19.04	4	9	16	26	41	61	84	110	140	175
				4	9	17	28	42	61	85	114	146	179
2_44	24.31	60.53	10.36	4	8	14	21	36	55	75	94	120	154
				4	8	16	20	34	64	72	96	128	146
2_46	24.45	57.04	12.91	4	8	14	24	36	48	64	90	118	136
				4	9	15	22	34	52	71	87	106	136
2_61	25.45	53.55	16.33	4	8	14	26	46	70	91	113	149	197
				4	10	19	30	45	68	94	122	152	186
2_22	26.31	64.37	9.70	4	7	11	18	28	42	56	68	85	111
				4	8	14	21	29	41	57	77	99	121
2_92	26.57	53.08	17.78	4	9	17	31	54	82	109	139	182	233
				4	11	22	35	55	82	110	146	188	230
2_13	26.62	61.44	12.04	4	6	15	28	34	60	69	96	126	142
				4	9	16	25	39	57	75	96	120	150
2_93	28.25	60.99	13.98	4	10	20	31	50	71	104	134	176	210
				4	9	18	30	48	70	94	134	180	213
2_12	29.67	65.74	12.11	4	6	15	20	30	50	67	90	115	126
				4	8	13	22	32	47	71	91	108	132

2_30	33.21	64.55	16.47	4	8	12	16	26	42	56	72	102	140
				4	8	13	20	30	41	56	80	111	138
2_94	33.62	58.11	21.34	4	9	18	31	55	88	121	157	194	236
				4	11	23	41	63	88	123	162	207	262
2_16	36.19	72.38	14.02	4	6	17	32	49	65	92	135	167	183
				4	11	20	28	50	81	102	117	159	222
2_34	36.28	76.83	11.03	4	8	13	19	26	38	55	74	95	115
				4	9	16	24	34	47	61	78	100	126
2_14	36.36	72.96	13.79	4	6	16	31	48	57	77	116	154	161
				4	11	19	26	42	70	93	103	128	182
2_98	37.01	63.95	20.69	4	9	18	33	51	72	105	147	184	230
				4	9	18	33	53	78	108	143	184	232
2_56	38.29	72.66	15.93	4	8	14	26	44	62	93	122	145	182
				4	11	19	29	47	68	94	123	155	193
2_116	43.29	71.75	21.56	4	11	22	39	65	96	134	175	223	280
				4	11	23	41	65	94	133	177	230	284
2_111	43.36	69.96	22.87	4	10	20	46	70	94	140	206	264	308
				4	12	25	47	74	108	155	203	262	334
2_18	44.29	89.79	10.06	4	7	10	14	17	24	37	48	57	70
				4	8	8	10	20	24	28	50	64	64
2_28	45.34	88.96	11.69	4	7	13	18	33	44	66	72	110	118
				4	8	12	21	30	50	58	82	98	138
2_15	46.13	89.89	11.83	4	12	10	28	52	34	84	124	74	172
				4	6	17	27	31	64	75	81	143	146
2_75	50.08	80.91	22.01	4	7	13	25	39	56	87	107	148	182
				4	8	14	25	40	59	84	110	147	180
2_29	50.83	93.06	14.34	4	10	18	30	45	59	103	165	219	314
				4	10	20	31	49	80	103	164	269	289
2_10	51.21	104.88	6.53	4	6	12	16	24	32	44	55	68	80
				4	6	12	17	24	31	44	55	68	82
2_5	52.01	104.95	7.28	4	5	9	14	13	16	26	34	36	44
				4	8	10	11	16	22	24	28	42	60
2_115	52.70	88.37	19.46	4	11	21	36	64	94	123	165	214	272
				4	11	23	40	63	91	126	167	213	265
2_7	53.66	105.42	8.60	4	5	10	20	26	24	44	80	98	93
				4	9	14	16	22	40	58	72	83	109
2_8	54.06	110.45	5.39	4	6	7	12	19	21	22	30	46	58
				4	8	12	13	16	22	30	36	44	56
2_6	56.38	102.26	13.51	4	5	10	19	22	25	40	62	80	90
				4	9	13	16	23	36	50	58	68	94
2_104	64.22	107.73	17.56	4	10	17	30	52	72	108	130	167	208
				4	11	20	33	52	76	105	138	173	213

2_105	65.06	106.55	19.22	4	6	9	15	28	43	65	92	134	172
				4	7	11	20	31	47	74	99	133	196
2_76	68.64	110.29	20.21	4	9	16	25	38	58	87	124	165	209
				4	10	20	34	53	78	109	146	191	245
2_63	73.83	116.23	21.28	4	8	14	27	50	80	114	153	200	258
				4	11	23	39	62	93	130	174	223	275
2_9	73.85	127.41	13.56	4	6	8	14	20	30	45	54	73	98
				4	7	10	14	22	34	42	58	78	94
2_60	79.89	131.67	16.65	4	8	14	26	45	68	93	125	171	223
				4	11	22	35	52	76	109	148	189	232
2_80	87.12	142.73	16.21	4	9	17	29	48	70	100	138	175	222
				4	11	20	36	58	81	112	146	189	240
2_42	104.27	164.99	17.94	4	8	14	21	32	48	67	91	117	149
				4	10	18	28	42	59	80	105	134	168
2_4	107.62	186.37	6.48	4	5	8	16	18	24	36	48	63	72
				4	8	10	15	22	26	38	54	64	80
2_36	166.29	262.64	12.30	4	8	13	20	29	41	56	72	89	110
				4	9	16	24	33	44	58	76	97	120
2_69	189.35	292.92	14.38	4	8	17	29	46	68	91	117	154	184
				4	9	17	28	49	69	92	119	151	184

Table 2. Space groups and unit cell dimensions of 109 hypothetical binodal zeolites, optimized as purely siliceous structures.

Structure	Space group symbol	Space group number	a [Å]	b [Å]	c [Å]	α [°]	β [°]	γ [°]
2_4	*Im-3m*	229	24.5550	24.5550	24.5550	90	90	90
2_5	*Im-3m*	229	23.6252	23.6252	23.6252	90	90	90
2_6	*Pn-3m*	224	19.2265	19.2265	19.2265	90	90	90
2_7	*P-43m*	215	14.0784	14.0785	14.0785	90	90	90
2_8	*Im-3m*	229	29.9045	29.9046	29.9046	90	90	90
2_9	*R-3m*	166	20.6871	20.6871	10.7470	90	90	120
2_10	*Im-3m*	229	30.8610	30.8610	30.8610	90	90	90
2_12	$I4_1/amd$	141	15.1769	15.1769	17.2033	90	90	90
2_13	*Fm-3m*	225	17.4521	17.4521	17.4521	90	90	90
2_14	*I4/mmm*	139	11.5929	11.5929	12.9540	90	90	90
2_15	*Pm-3n*	223	13.6367	13.6367	13.6367	90	90	90
2_16	$P4_2/mnm$	136	10.2171	10.2171	16.3964	90	90	90
2_17	*Im-3m*	229	31.6666	31.6666	31.6666	90	90	90
2_18	*Im-3m*	229	18.1332	18.1332	18.1332	90	90	90
2_19	*Im-3m*	229	26.0211	26.0211	26.0211	90	90	90
2_20	*Pm-3m*	221	17.5191	17.5191	17.5191	90	90	90
2_21	*Fm-3m*	225	31.5256	31.5256	31.5256	90	90	90
2_22	*Pm-3m*	221	19.5087	19.5087	19.5087	90	90	90
2_23	*Fm-3m*	225	32.8255	32.8255	32.8255	90	90	90
2_24	*Pm-3m*	221	14.6896	14.6986	14.6896	90	90	90
2_25	*Fm-3m*	225	30.1897	30.1897	30.1897	90	90	90
2_26	*Fm-3m*	225	30.2151	30.2151	30.2151	90	90	90
2_27	*Fm-3m*	225	27.5480	27.548	27.5480	90	90	90
2_28	*Im-3*	204	16.0155	16.0155	16.0155	90	90	90
2_29	*Fd-3c*	228	29.9172	29.9172	29.9172	90	90	90
2_30	*Pn-3m*	224	15.3879	15.3879	15.3879	90	90	90
2_31	*R-3m* (*Fd-3m*)	166 *(227)*	26.3028	26.3028	64.9314	90	90	120
2_32	*Im-3m*	229	24.9270	24.9270	24.9270	90	90	90
2_33	*R-3m*	166	13.1741	13.1741	32.3570	90	90	120
2_34	*Im-3m*	229	25.9183	25.9183	25.9183	90	90	90
2_35	*Fd-3m*	227	30.8413	30.8416	30.8413	90	90	90
2_36	*Pm-3m*	221	19.8342	19.8342	19.8342	90	90	90
2_37	*Pn-3m*	224	19.6887	19.6887	19.6887	90	90	90
2_39	*P1* (*Im-3m*)	1 *(229)*	21.5940	21.6260	21.6370	90.1262	89.9558	90.0775
2_40	*R-3m*	166	13.2084	13.2084	23.8034	90	90	120
2_41	*Im-3m*	229	25.2127	25.2127	25.2127	90	90	90
2_42	*Im-3m*	229	20.0209	20.0209	20.0209	90	90	90
2_43	*Fm-3m*	225	25.9040	25.9040	25.9040	90	90	90
2_44	*P-43m*	215	11.3123	11.3124	11.3124	90	90	90
2_45	*Pm-3m*	221	17.6786	17.6786	17.6786	90	90	90
2_46	*Pn-3m*	224	15.4919	15.4919	15.4919	90	90	90
2_47	*Pm-3m*	221	19.0003	19.0003	19.0003	90	90	90
2_48	*Pm-3n*	223	16.7613	16.7613	16.7613	90	90	90
2_50	*P-31m*	162	12.3351	12.3351	8.6007	90	90	120
2_51	$P6_3/mcm$	193	12.3340	12.3340	17.2043	90	90	120

2_52	*Pn*-3*m*	224	16.7584	16.7584	16.7584	90	90	90
2_53	*Pn*-3*m*	224	18.5448	18.5448	18.5448	90	90	90
2_54	*I*4/*mmm*	139	14.8438	14.8438	20.0782	90	90	90
2_55	$P6_3/mcm$	193	13.7562	13.7562	19.2727	90	90	120
2_56	*P*-31*m*	162	13.7003	13.7003	9.2686	90	90	120
2_57	*I*4/*mmm*	139	14.0993	14.0993	15.5435	90	90	90
2_58	*I*4/*mmm*	139	13.5265	13.5265	20.6385	90	90	90
2_59	*P*4/*nmm*	129	13.5133	13.5133	10.3319	90	90	90
2_60	*Im*-3*m*	229	17.9320	17.9320	17.9320	90	90	90
2_61	$I4_1/amd$	141	16.3875	16.3875	10.9441	90	90	90
2_62	*Pm*-3*m*	221	14.5985	14.5985	14.5985	90	90	90
2_63	*I*-4*m*2	119	12.6142	12.6142	9.4486	90	90	90
2_64	*Pm*-3*m*	221	18.3419	18.3419	18.3419	90	90	90
2_65	*Ia*-3	206	18.0311	18.0311	18.0311	90	90	90
2_67	*Ia*-3*d*	230	19.9520	19.9520	19.9520	90	90	90
2_68	$I4_1/amd$	141	15.1043	15.1043	10.7274	90	90	90
2_69	*R*-3*m*	166	16.6853	16.6853	20.9554	90	90	120
2_70	*Pm*-3*m*	221	13.8940	13.8940	13.8940	90	90	90
2_71	$P2_13$	198	14.0298	14.0298	14.0298	90	90	90
2_73	*Fd*-3*m*	227	29.6184	29.6184	29.6184	90	90	90
2_74	*Fm*-3*m*	225	30.4872	30.4872	30.4872	90	90	90
2_75	*Fd*-3*m*	227	25.9368	25.9368	25.9368	90	90	90
2_76	*P*-43*m*	215	13.3418	13.3418	13.3418	90	90	90
2_77	*Pn*-3*m*	224	15.5787	15.5787	15.5787	90	90	90
2_78	$P6_3/mmc$	194	13.5479	13.5479	19.3503	90	90	120
2_79	*Im*-3*m*	229	21.2424	21.2424	21.2424	90	90	90
2_80	*Im*-3*m*	229	18.0938	18.0938	18.0938	90	90	90
2_81	*I*4/*mmm*	139	13.9993	13.9993	10.2051	90	90	90
2_82	*Pn*-3*m*	224	15.8240	15.8240	15.8240	90	90	90
2_83	*R*-3*m*	166	12.9786	12.9786	22.4610	90	90	120
2_84	$P6_3/mmc$	194	12.9887	12.9887	14.9436	90	90	120
2_85	*I*4/*mmm*	139	13.2812	13.2812	15.4875	90	90	90
2_86	*P*-3*m*1	164	12.7931	12.7931	10.0490	90	90	120
2_87	$P6_3/mmc$	194	12.7982	12.7982	20.0706	90	90	120
2_88	*P*4/*nmm*	129	13.5200	13.5199	7.6115	90	90	90
2_89	$P6_3/mmc$	194	12.9122	12.9122	15.1051	90	90	120
2_90	*R*-3*m*	166	12.7260	12.7259	30.3678	90	90	120
2_91	*I*4/*mcm*	140	13.9768	13.9768	19.1953	90	90	90
2_92	*P*4/*nbm*	125	13.9490	13.9490	9.2497	90	90	90
2_93	*Im*3*m*	229	17.2697	17.2697	17.2697	90	90	90
2_94	*C*2 (*Fd*-3*m*)	5 *(227)*	29.4382	29.3841	20.7989	90	90	90
2_95	*I*4/*mmm*	139	12.2058	12.2058	19.1794	90	90	90
2_96	*Im*-3	204	16.4413	16.4413	16.4413	90	90	90
2_97	*Pm*3*n*	223	16.1973	16.1973	16.1973	90	90	90
2_98	$P4_132$	213	11.5642	11.5642	11.5642	90	90	90
2_99	*Pm*3	200	12.8171	12.8171	12.8171	90	90	90
2_100	*I*-4*m*2	119	12.8690	12.8691	7.6292	90	90	90
2_101	*Fm*3*m*	225	13.4592	13.4592	13.4592	90	90	90
2_102	*R*-3*m*	166	12.6141	12.6141	16.6417	90	90	120
2_103	$P6_3/mcm$	193	13.6152	13.6152	13.9813	90	90	120

2_104	*P*-31*m*	162	13.4810	13.4810	6.5129	90	90	120
2_105	*P*1 (*R*-3*c*)	1 *(167)*	10.6747	16.8789	16.9018	67.8079	86.0781	86.1532
2_106	$P6_3/mmc$	194	12.4093	12.4093	15.4571	90	90	120
2_107	$P6_3/mmc$	194	12.3972	12.3972	10.3205	90	90	120
2_108	*R*-3*m*	166	12.4186	12.4186	30.8573	90	90	120
2_109	*Pn*-3*m*	224	17.2562	17.2562	17.2562	90	90	90
2_110	*R*-3*m*	166	12.4060	12.4060	23.1948	90	90	120
2_111	$P4_132$	213	11.6324	11.6324	11.6324	90	90	90
2_112	$P2_13$	198	13.7019	13.7019	13.7019	90	90	90
2_113	*Fddd*	70	7.4170	13.5469	23.6645	90	90	90
2_114	*I*4/*mcm*	140	13.7055	13.7055	14.1225	90	90	90
2_115	*P*4/*nbm*	125	13.4128	13.4128	6.8567	90	90	90
2_116	*I*432	211	16.4510	16.4519	16.4510	90	90	90
2_117	$P4_2/mnm$	136	7.1839	7.1839	12.4079	90	90	90

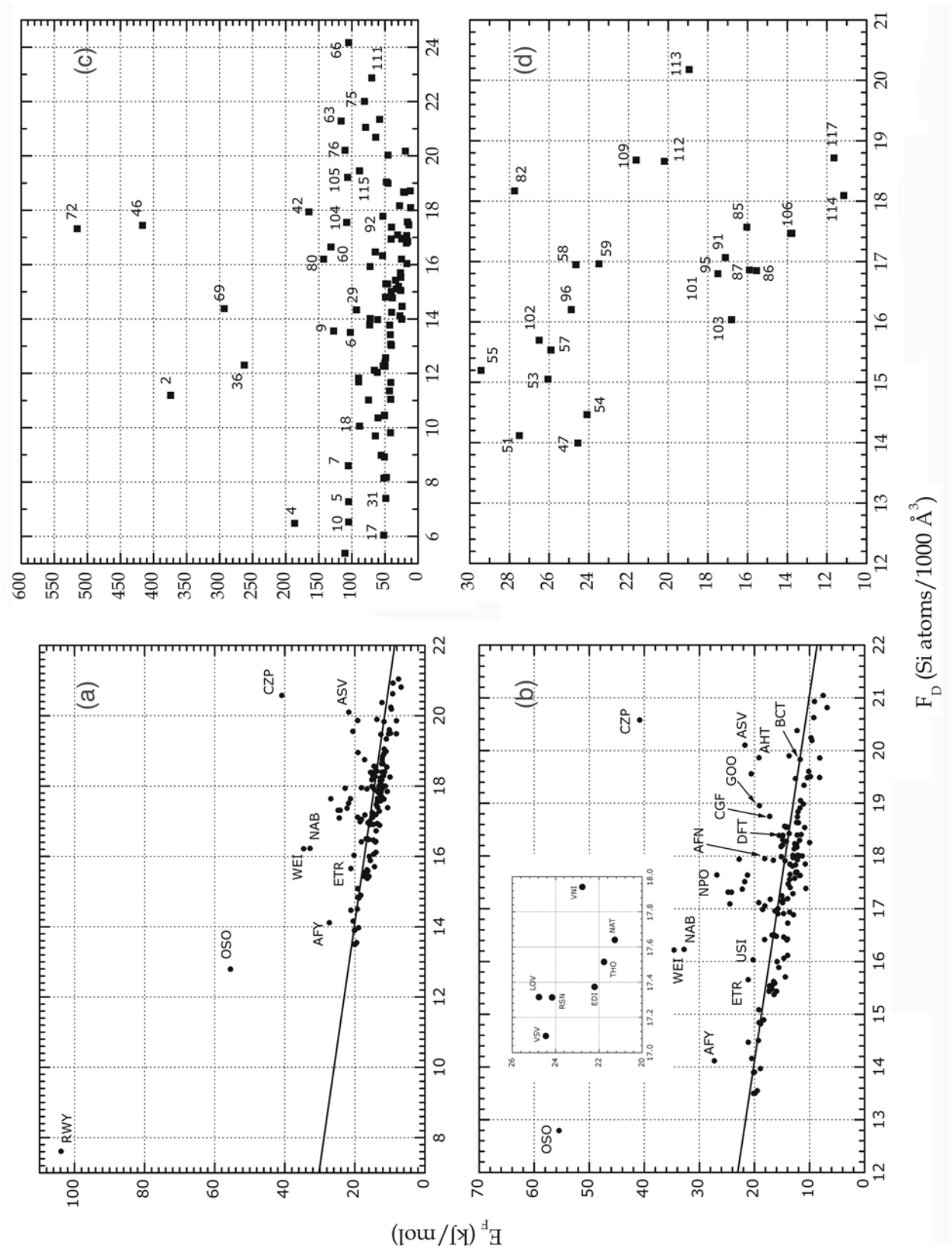

Figure 1. Framework energy, E_F (kJ/mol), with respect to α-quartz, versus framework density (Si atoms per 1000 Å^3) for **(a)** and **(b)** all known zeolitic structure types; **(b)** and **(d)** hypothetical binodal zeolitic structures.

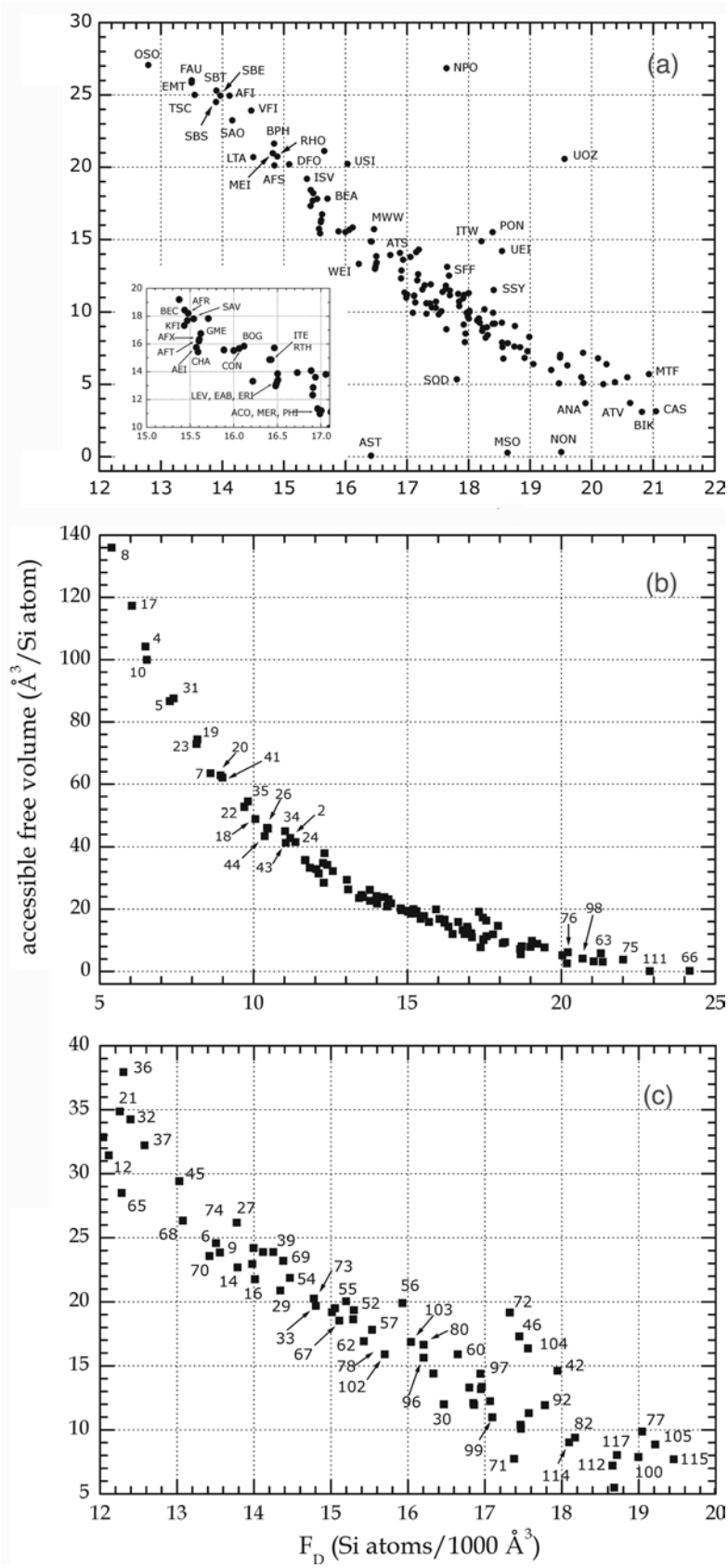

Figure 2. Accessible volume (Å^3 per Si atom) versus framework density for **(a)** all known zeolitic structure types; **(b)** hypothetical binodal zeolitic structures. Inset in **(b)** shows structures with accessible volumes below 30 Å^3 per Si atom.

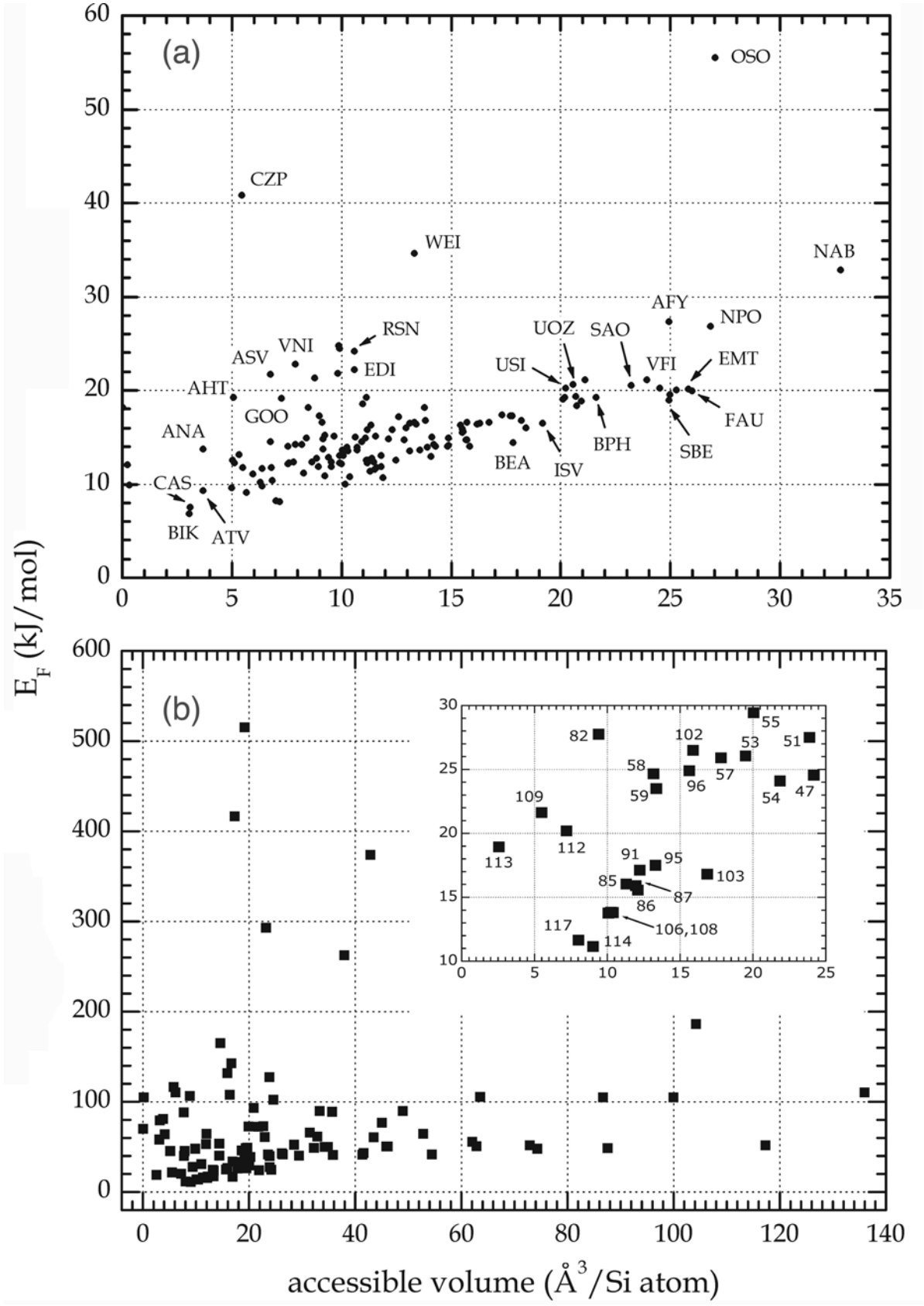

Figure 3. Framework energy with respect to α-quartz versus accessible volume (Å^3 per Si atom) for **(a)** all known zeolitic structure types; **(b)** and **(c)** hypothetical binodal zeolitic structures. Hypothetical structures of particular chemical interest are identified in **(c)**.

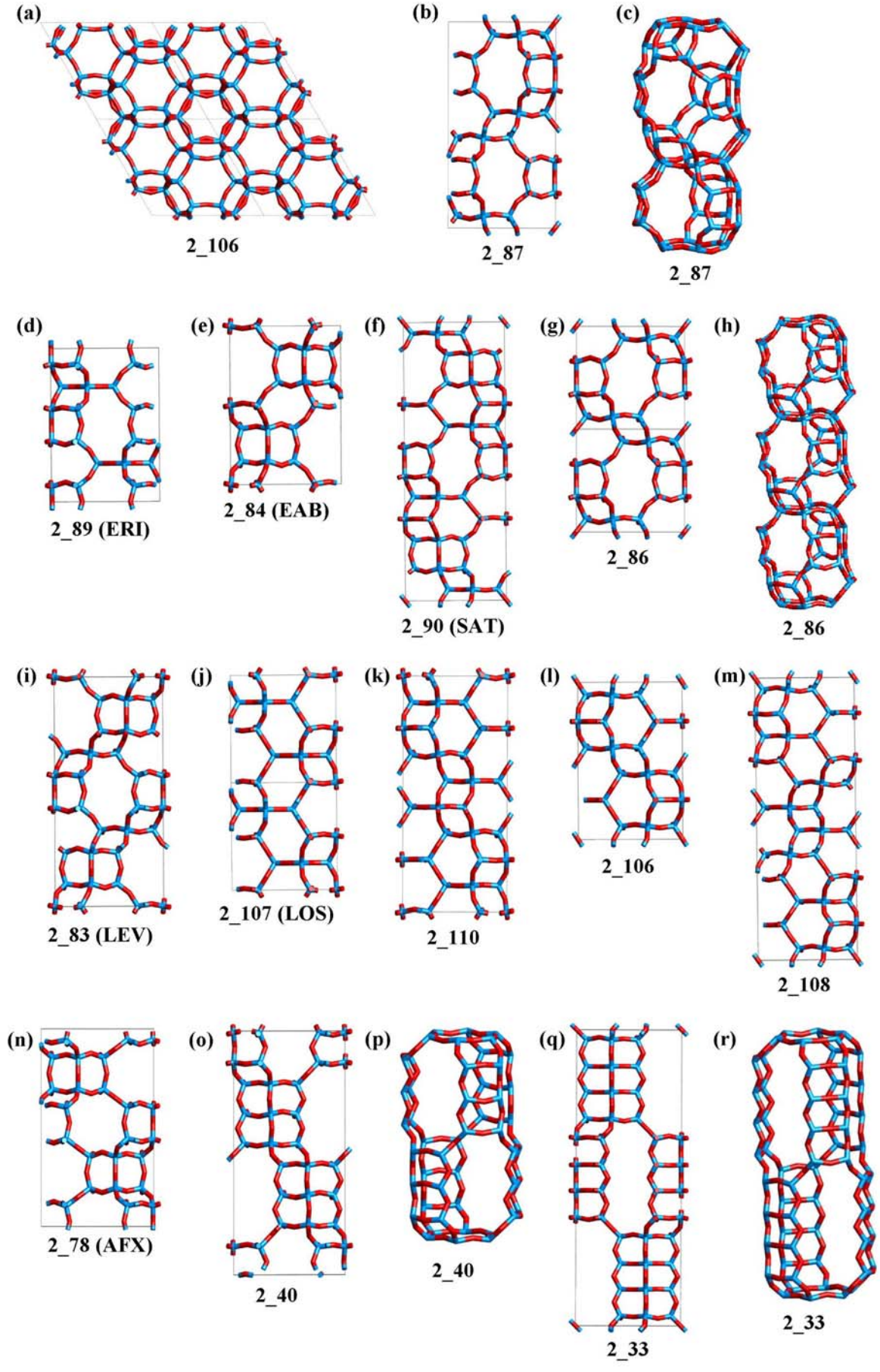

Figure 4. Molecular graphic illustrations of structures from the ABC-6 family.

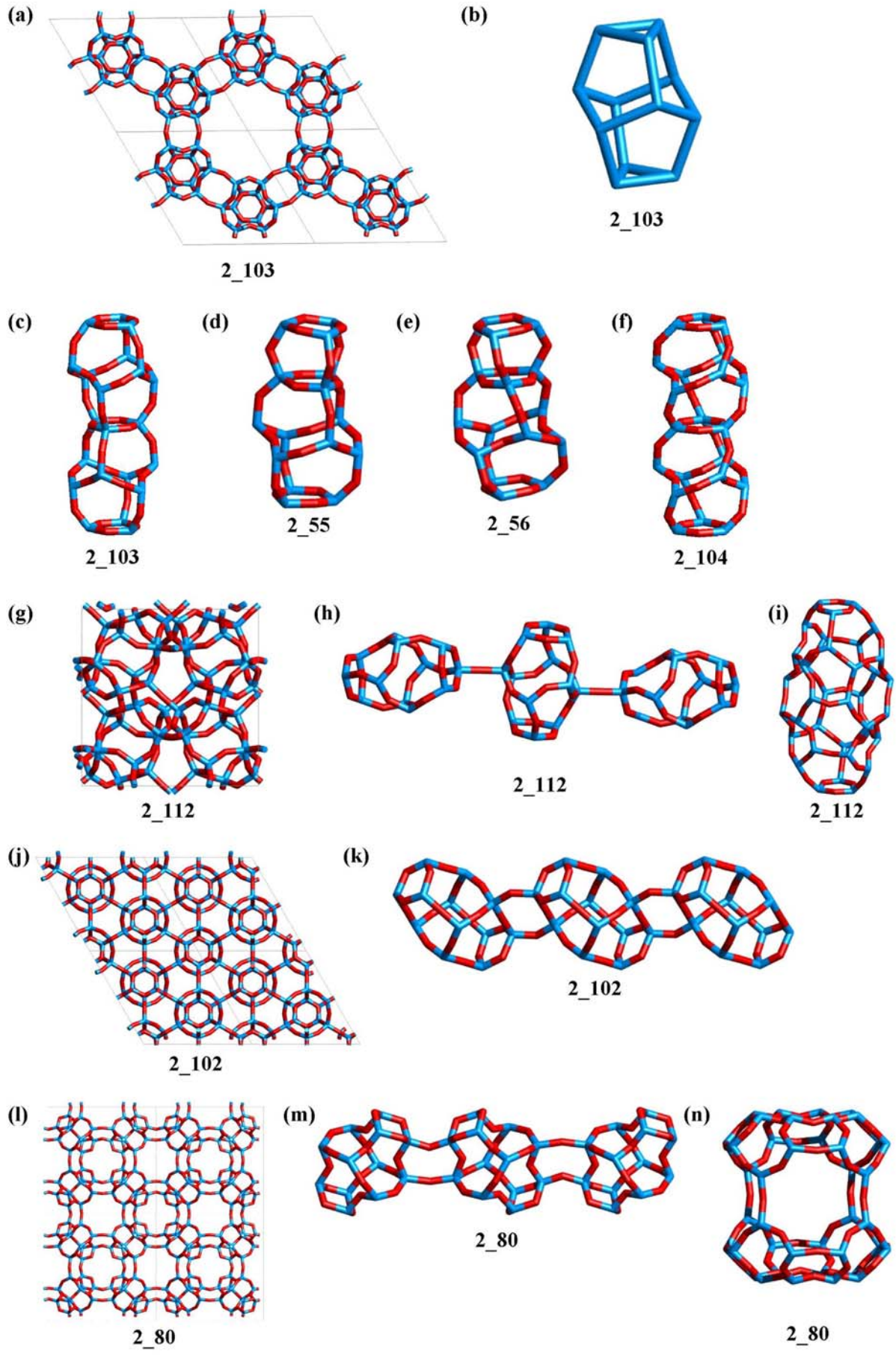

Figure 5. Molecular graphic illustrations of structures from the [$3^2 5^6$] family.

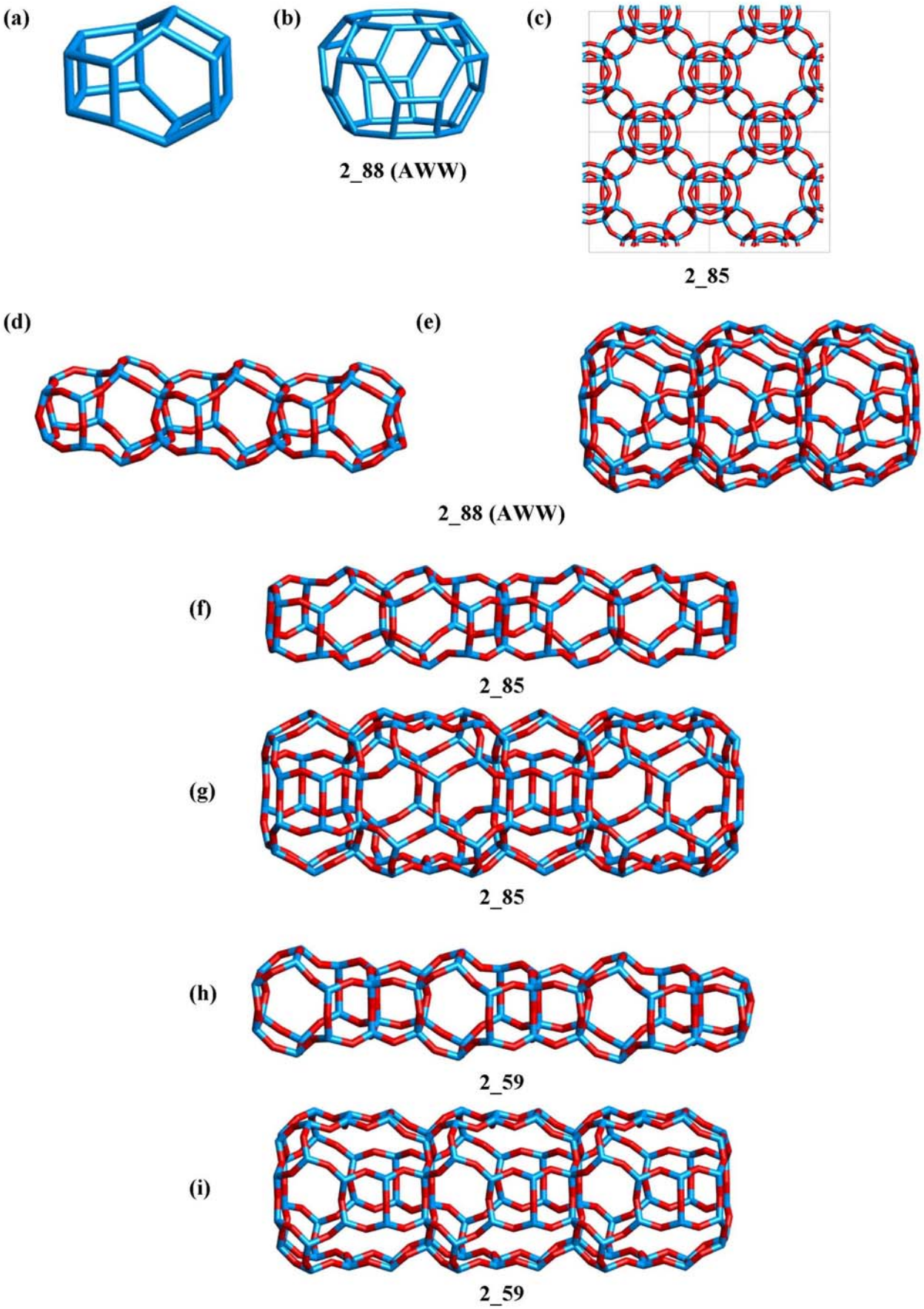

Figure 6. Molecular graphic illustrations of structures from the AWW family.

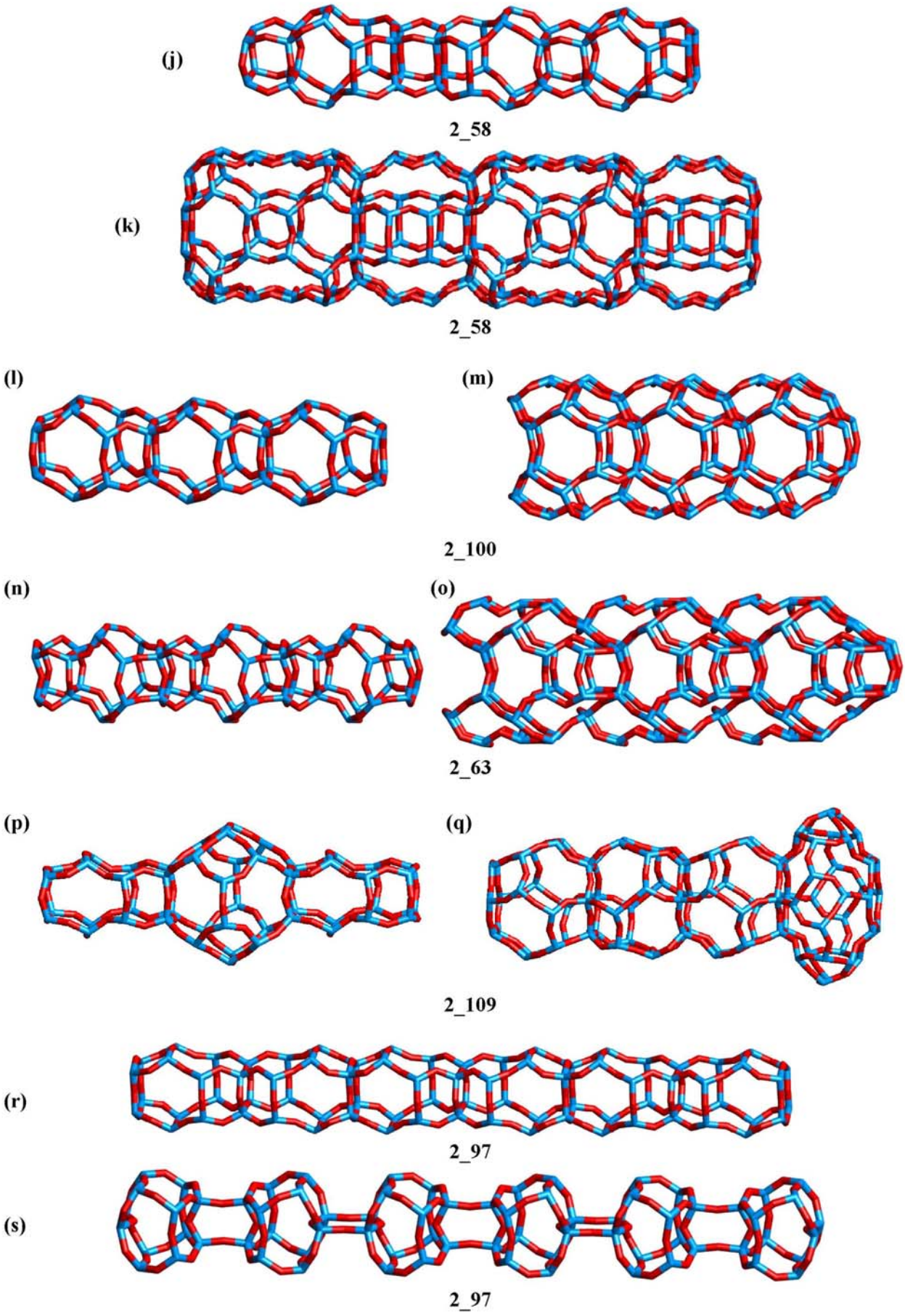

Figure 6. (cont.)

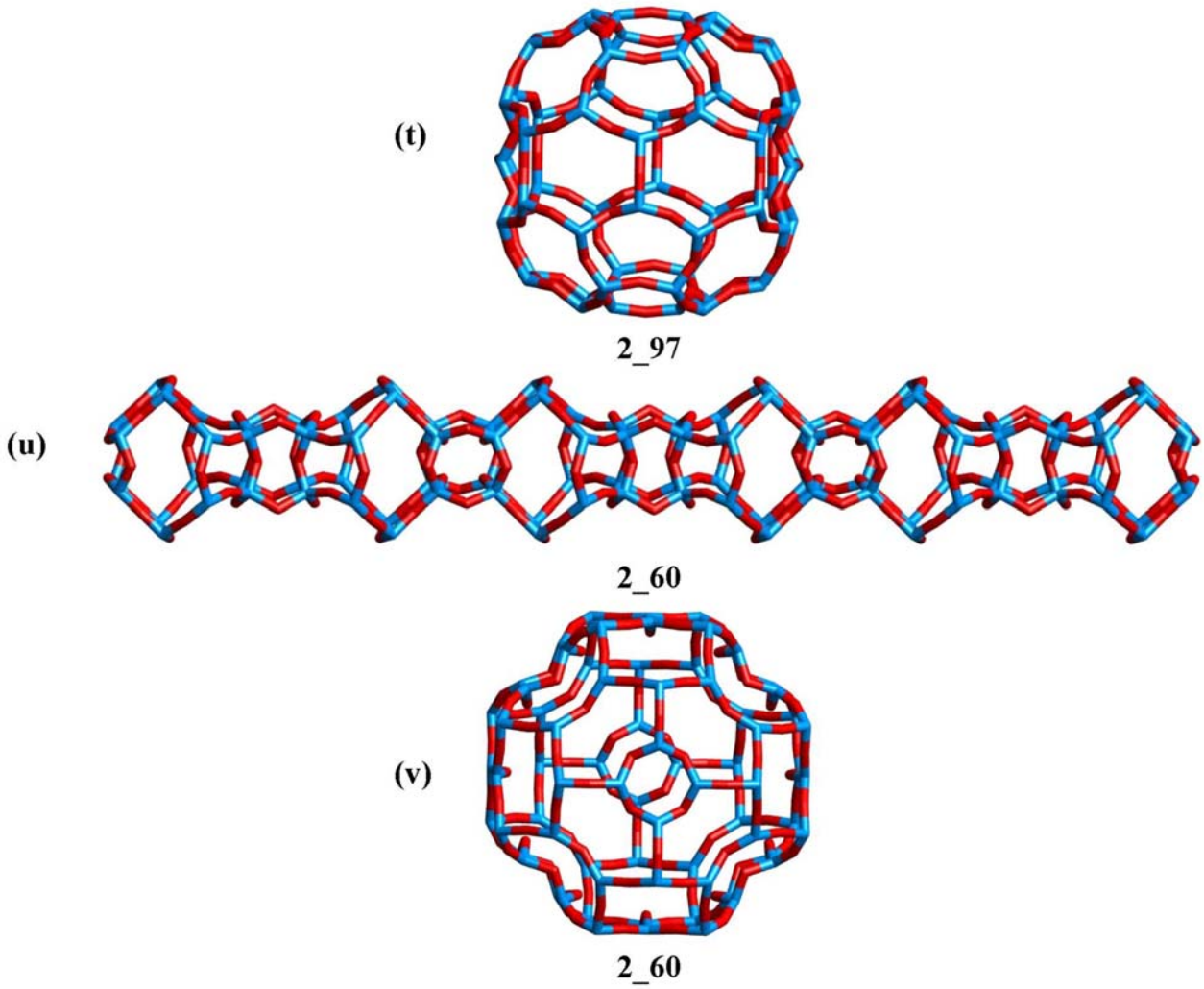

Figure 6. (cont.)

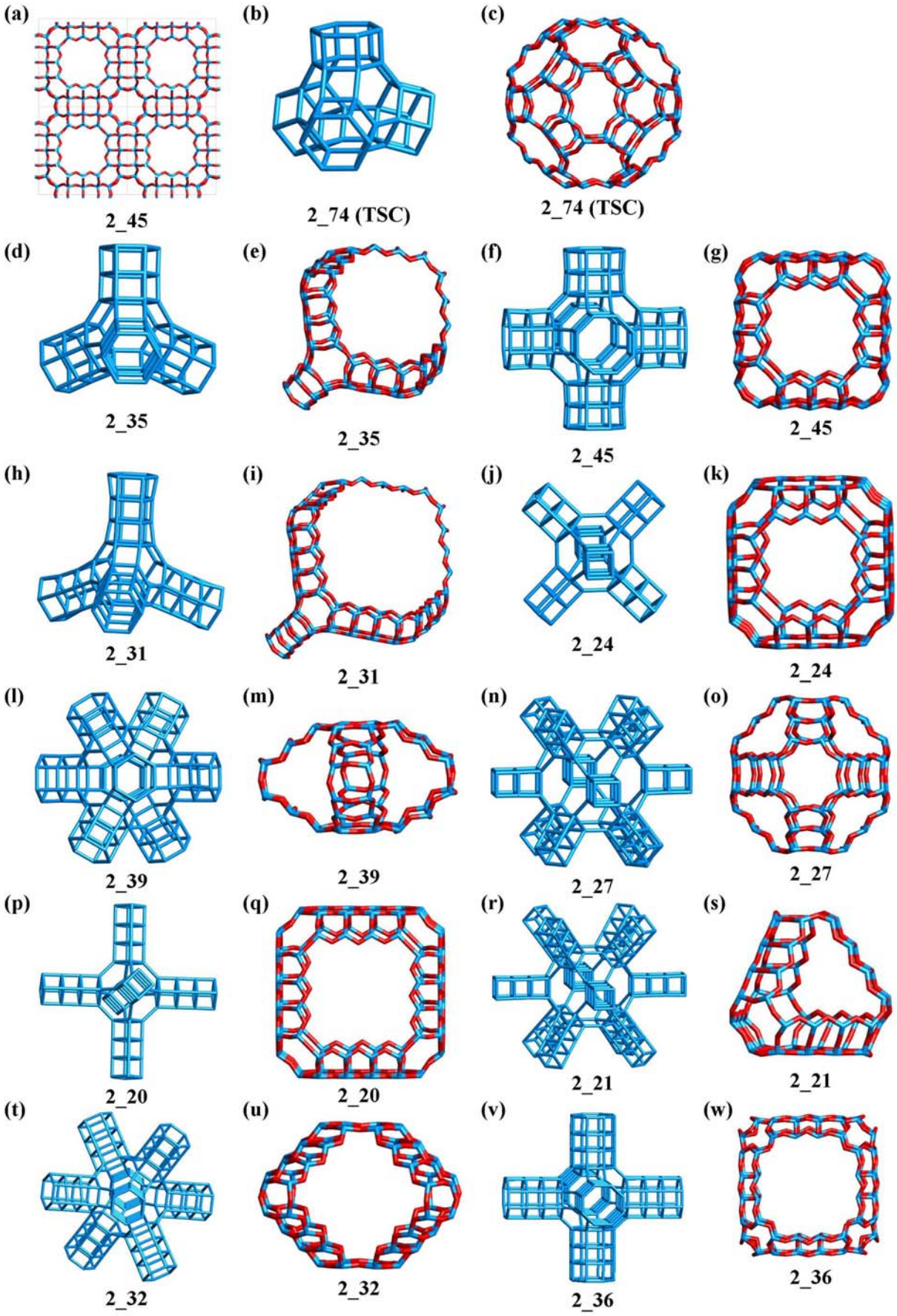

Figure 7. Molecular graphic illustrations of structures from the Supercage family.

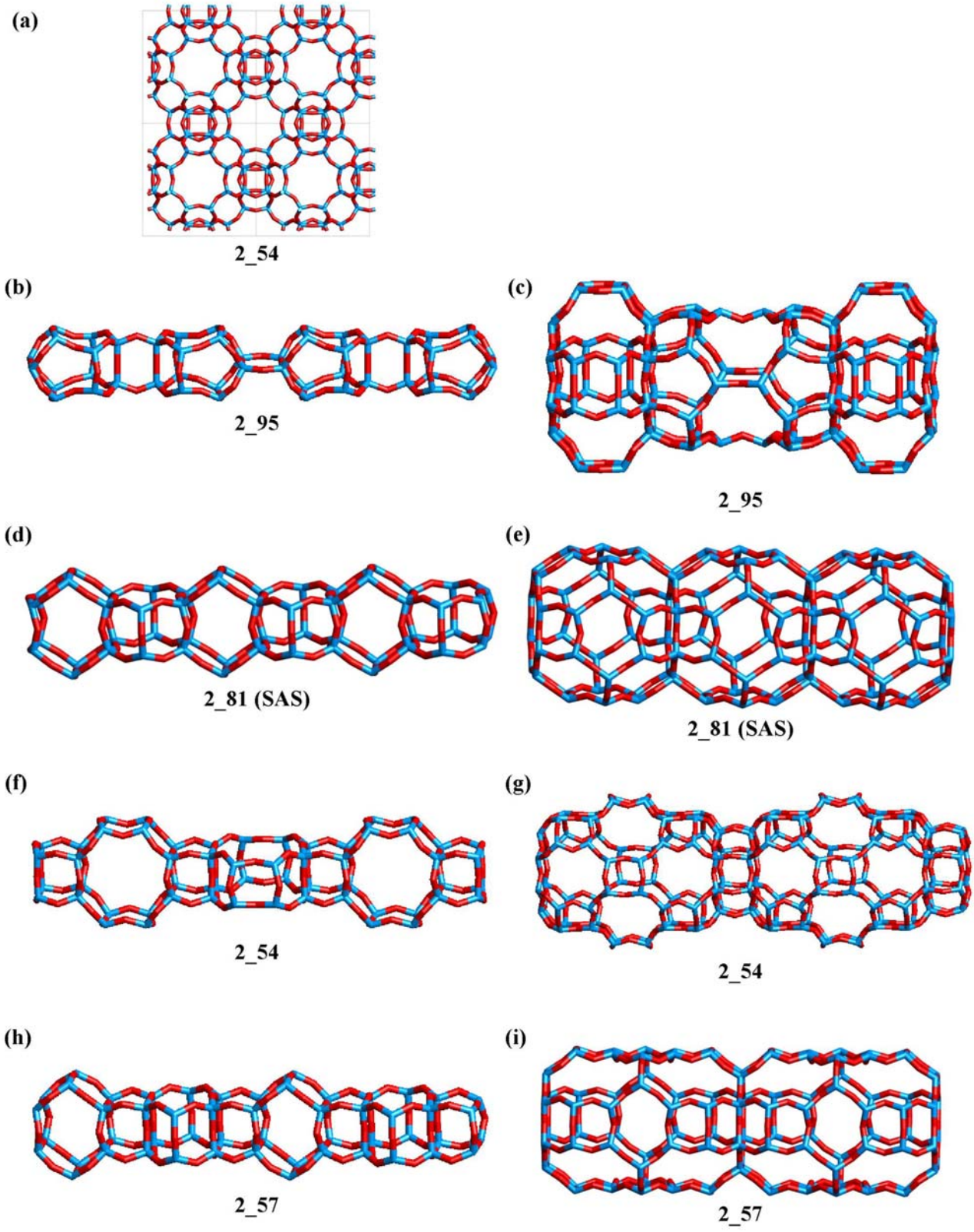

Figure 8. Molecular graphic illustrations of structures from the SAS family.

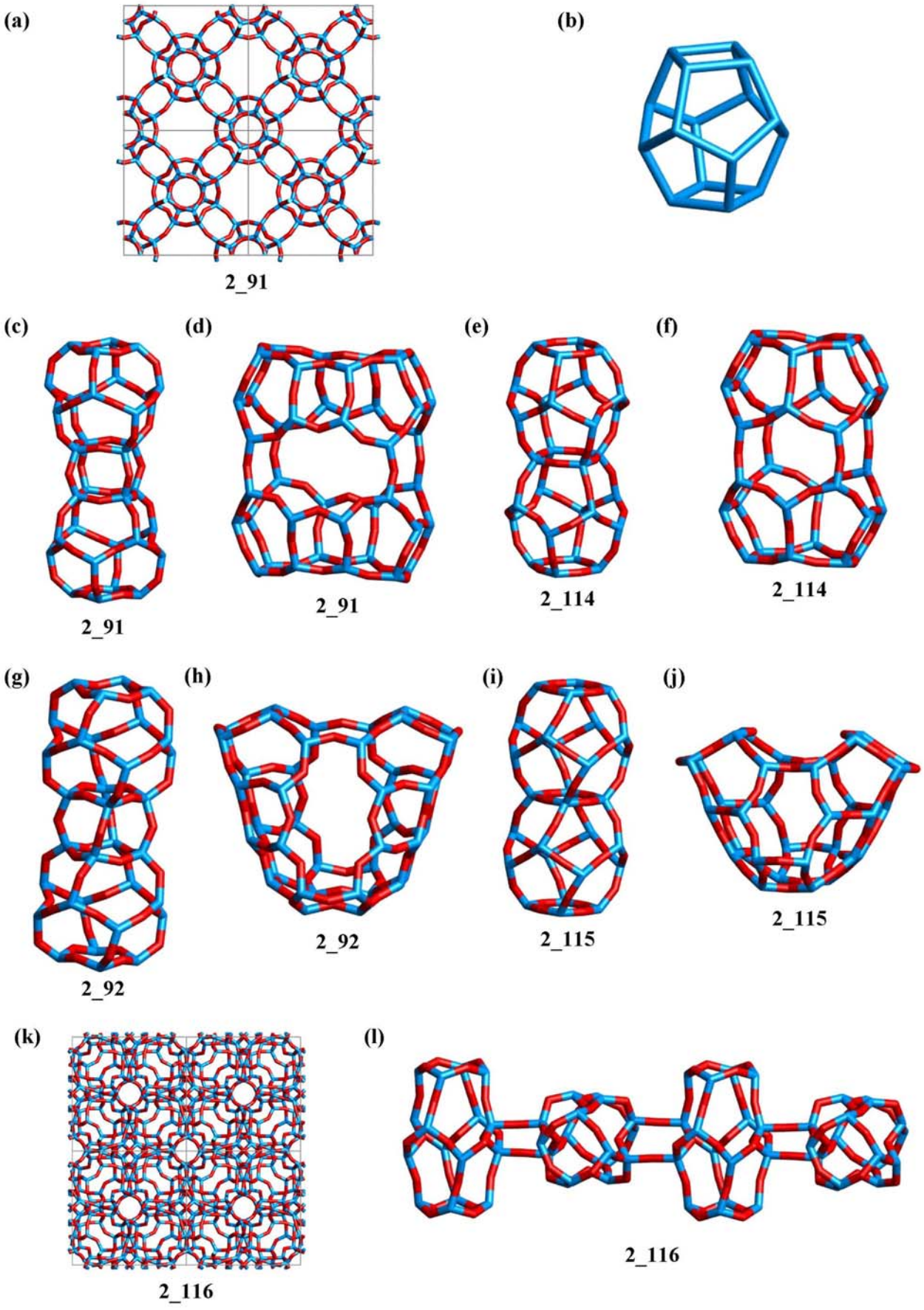

Figure 9. Molecular graphic illustrations of structures from the [$4^2 5^8$] family.

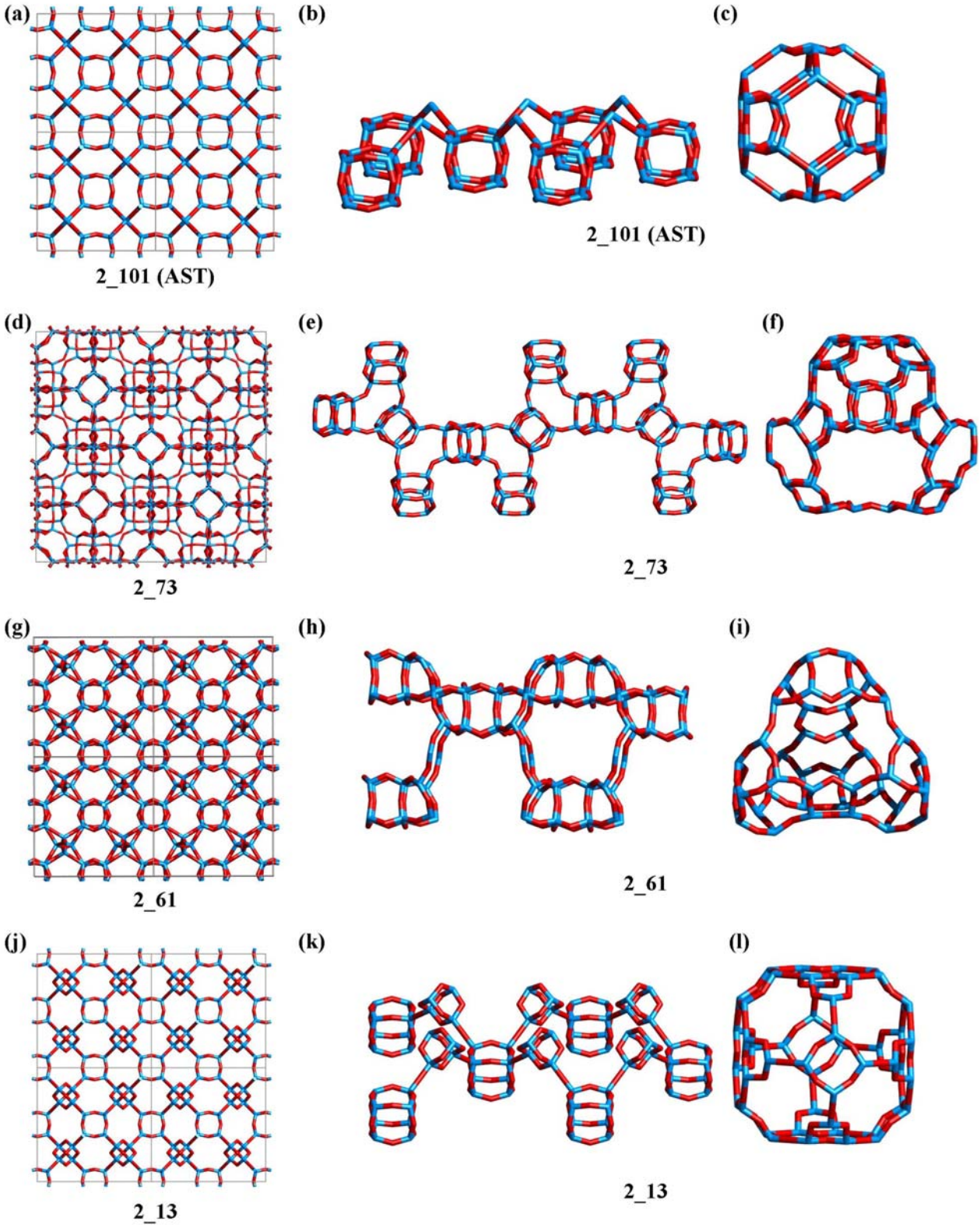

Figure 10. Molecular graphic illustrations of structures from the AST family.

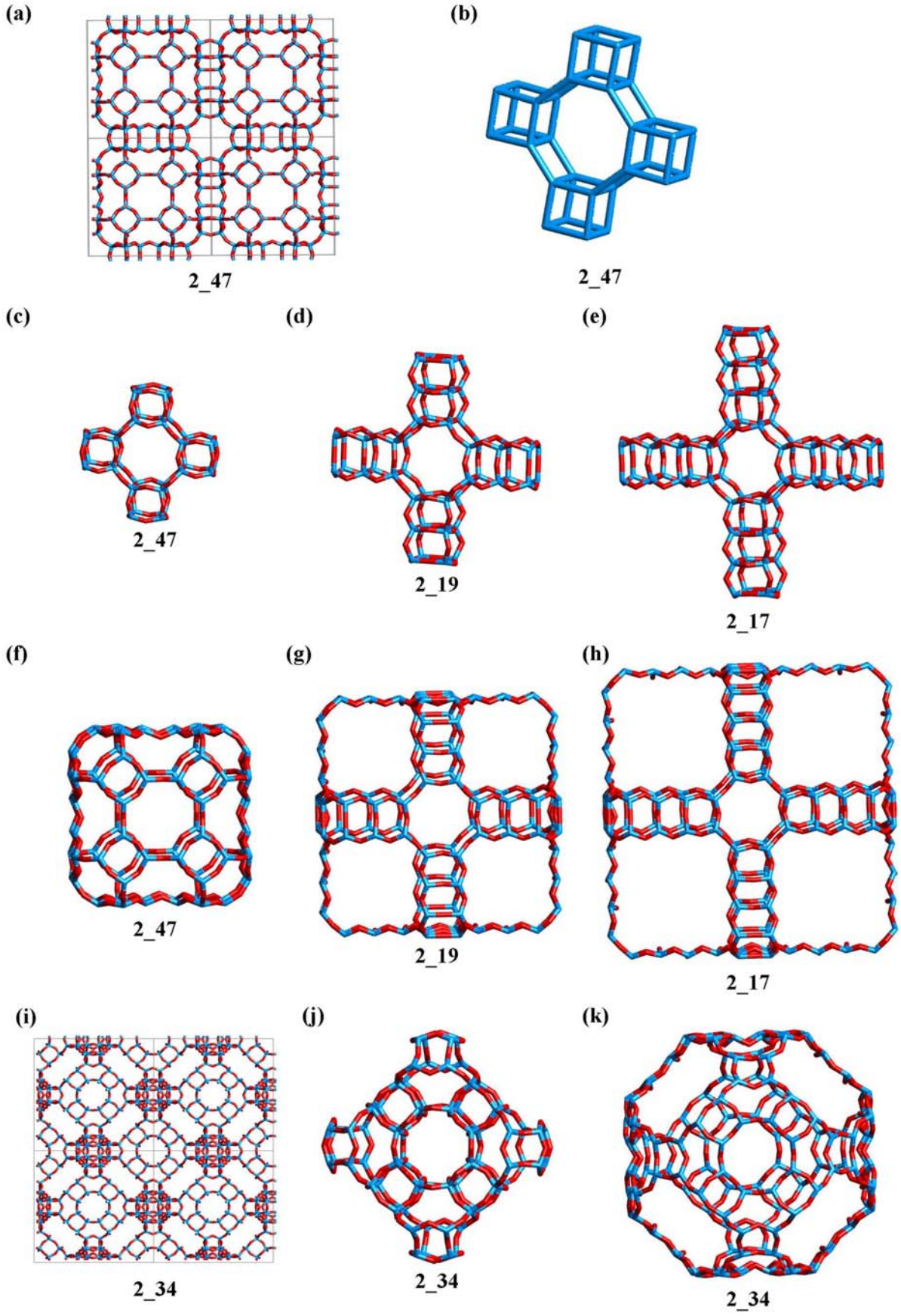

Figure 11. Molecular graphic illustrations of structures from the D8R family.

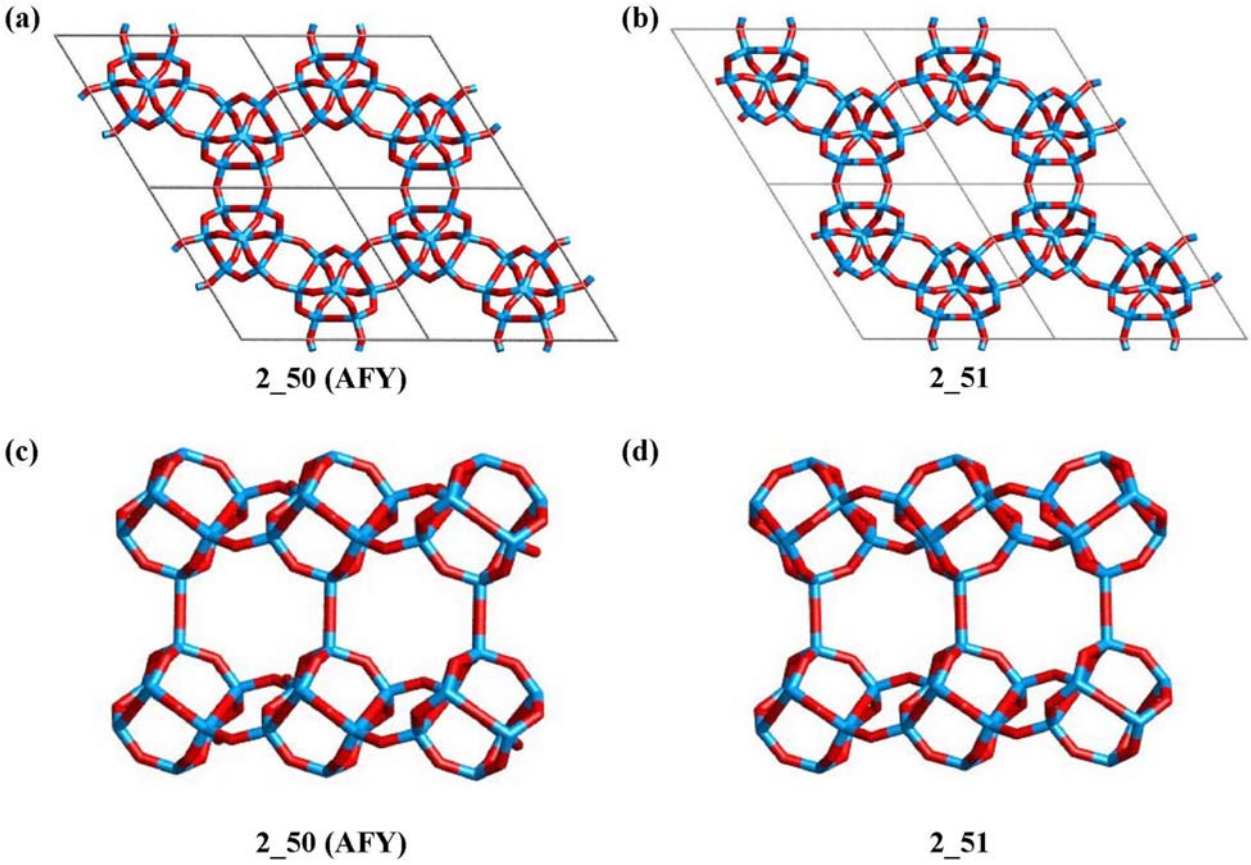

Figure 12. Molecular graphic illustrations of structures from the AFY family.

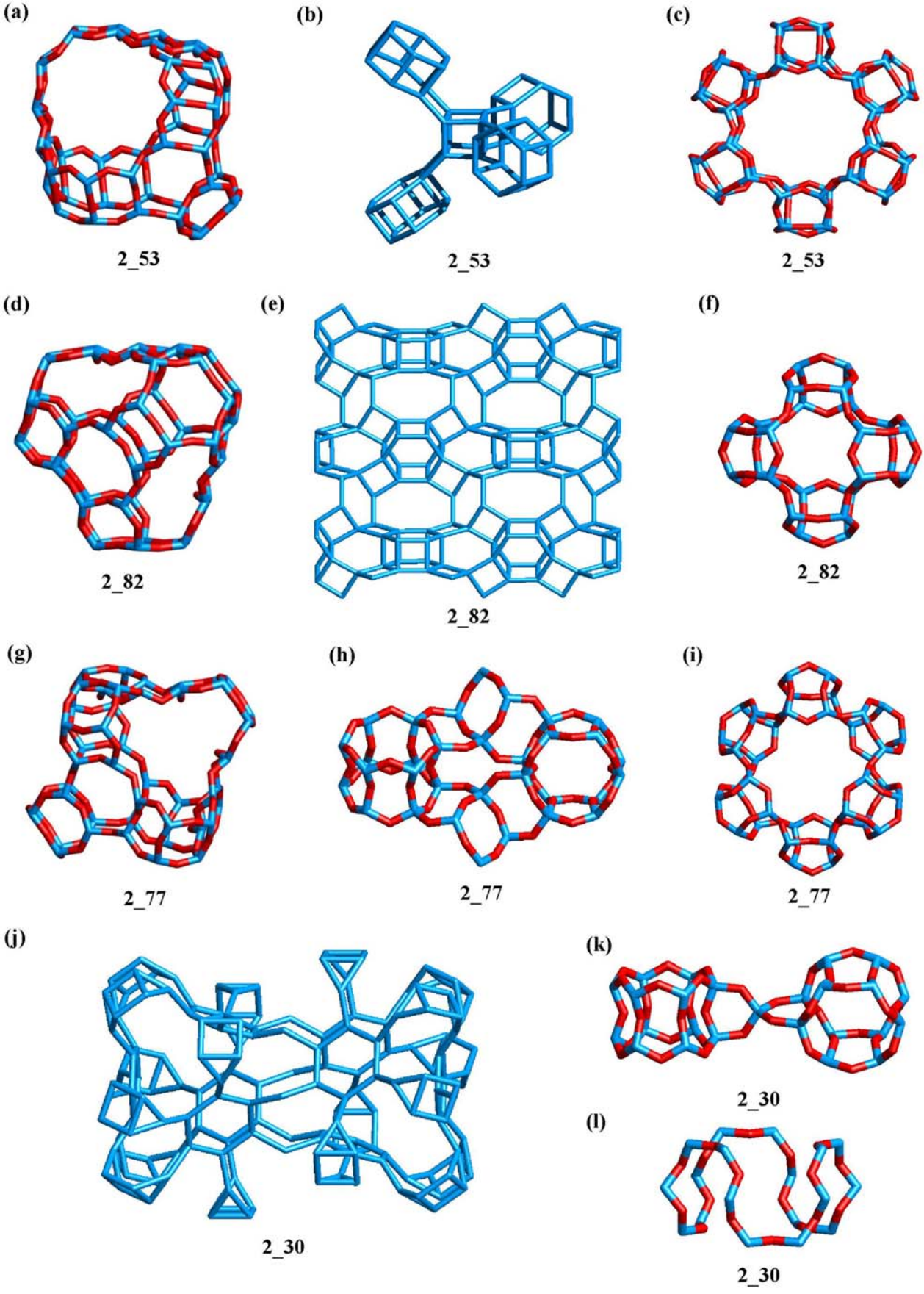

Figure 13. Molecular graphic illustrations of structures from the D6R family.

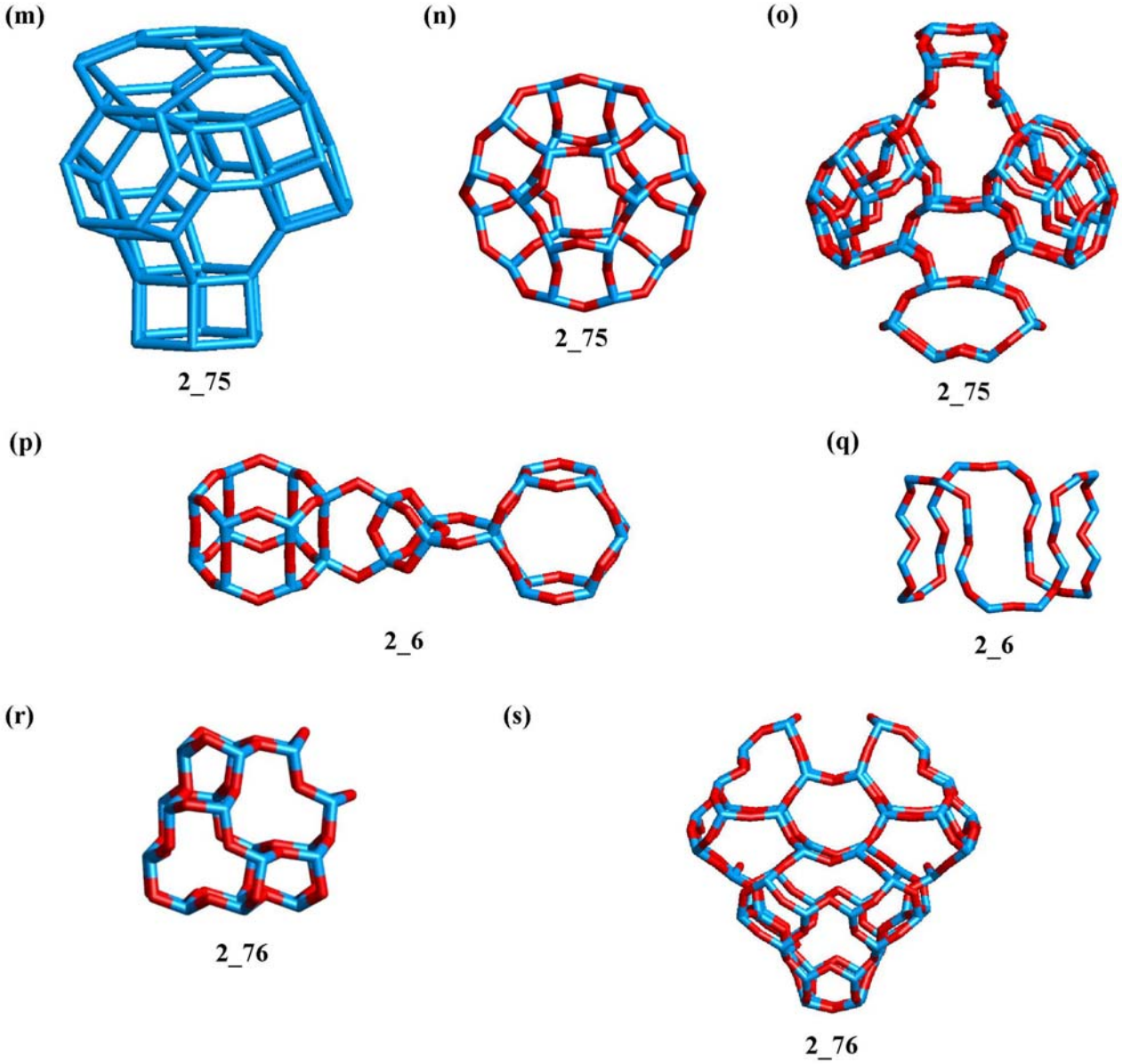

Figure 13. (Cont.)

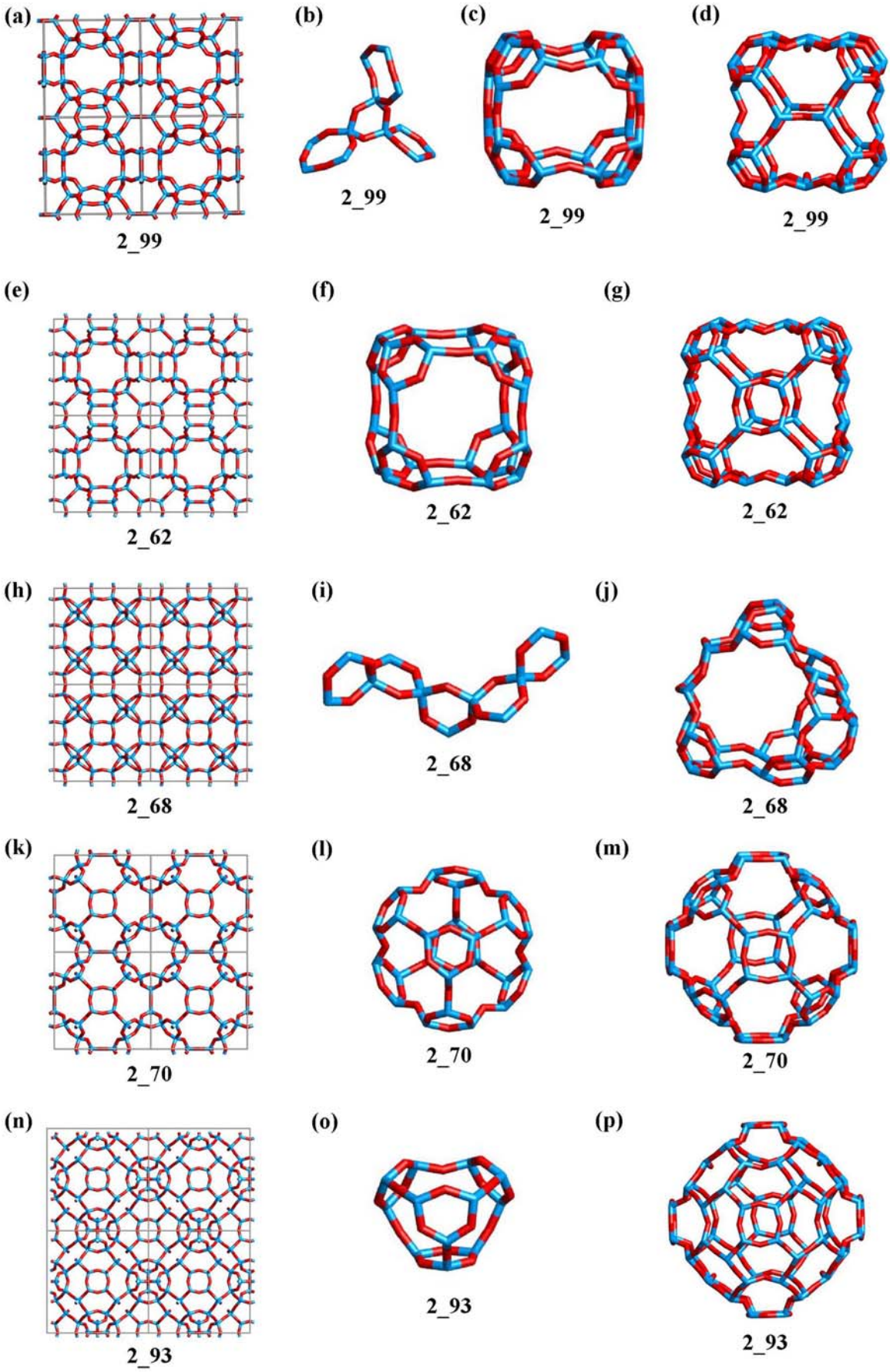

Figure 14. Molecular graphic illustrations of structures from the 3 and 4-ring family.

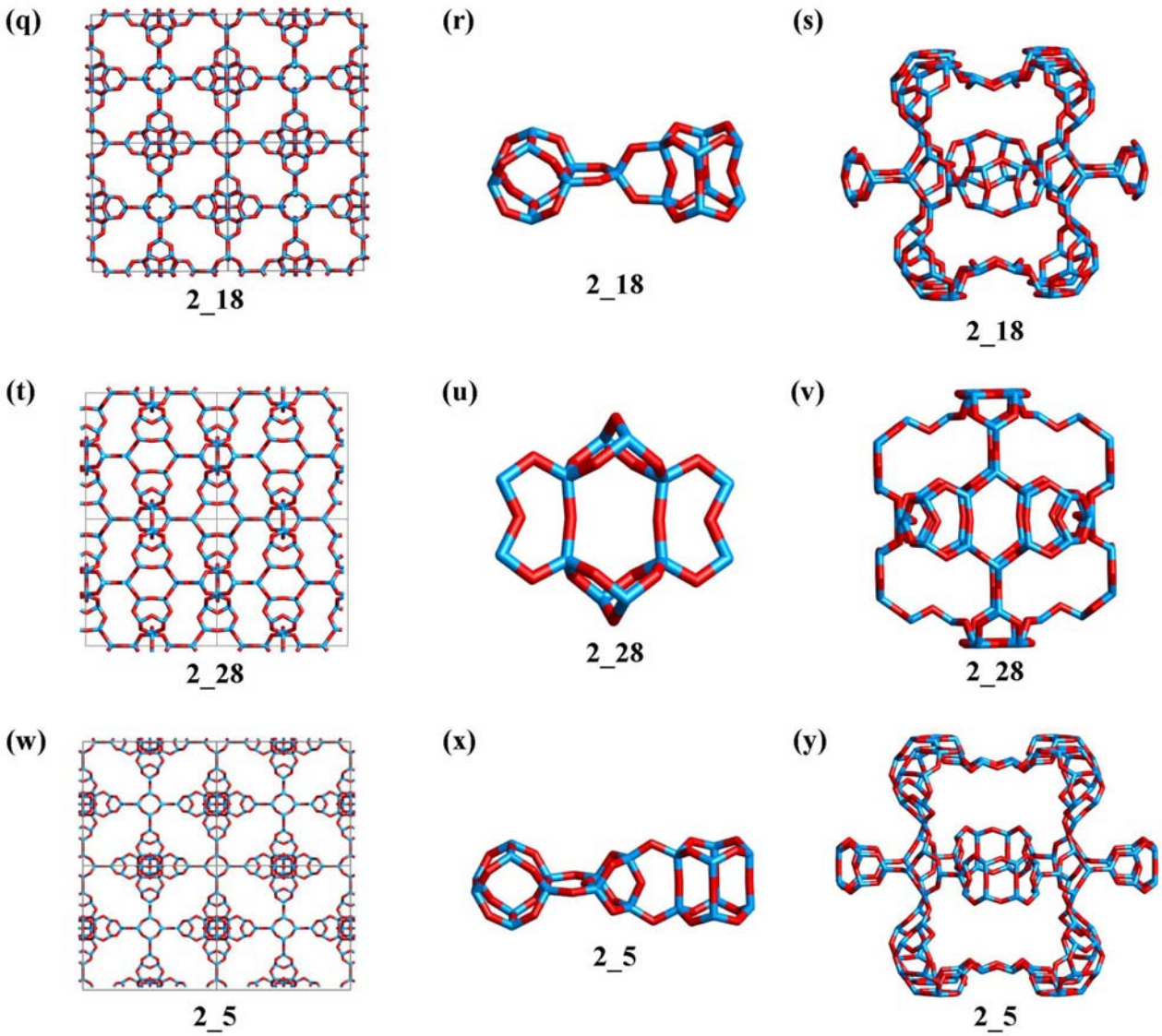

Figure 14. (Cont.)

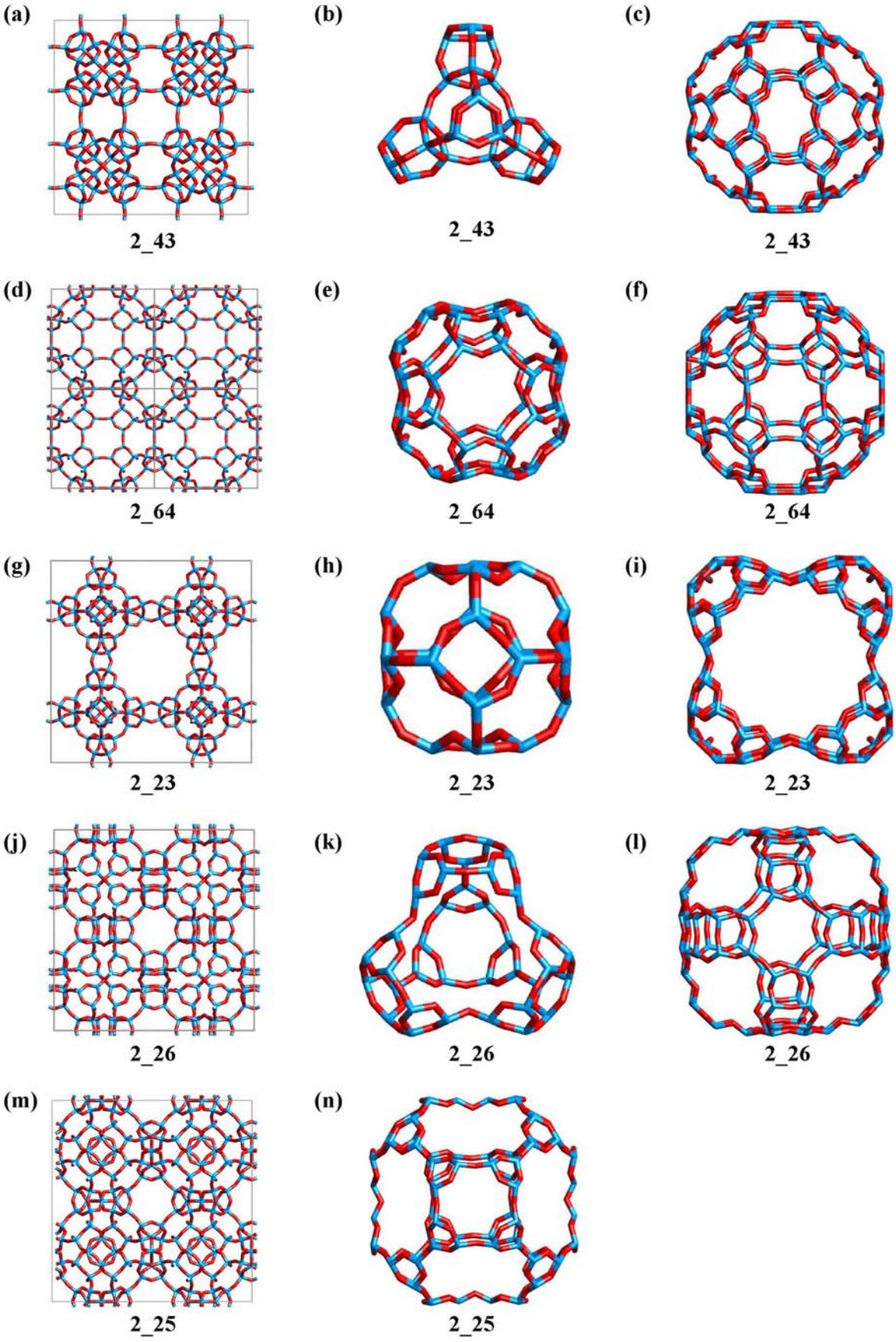

Figure 15. Molecular graphic illustrations of structures from the D3R family.

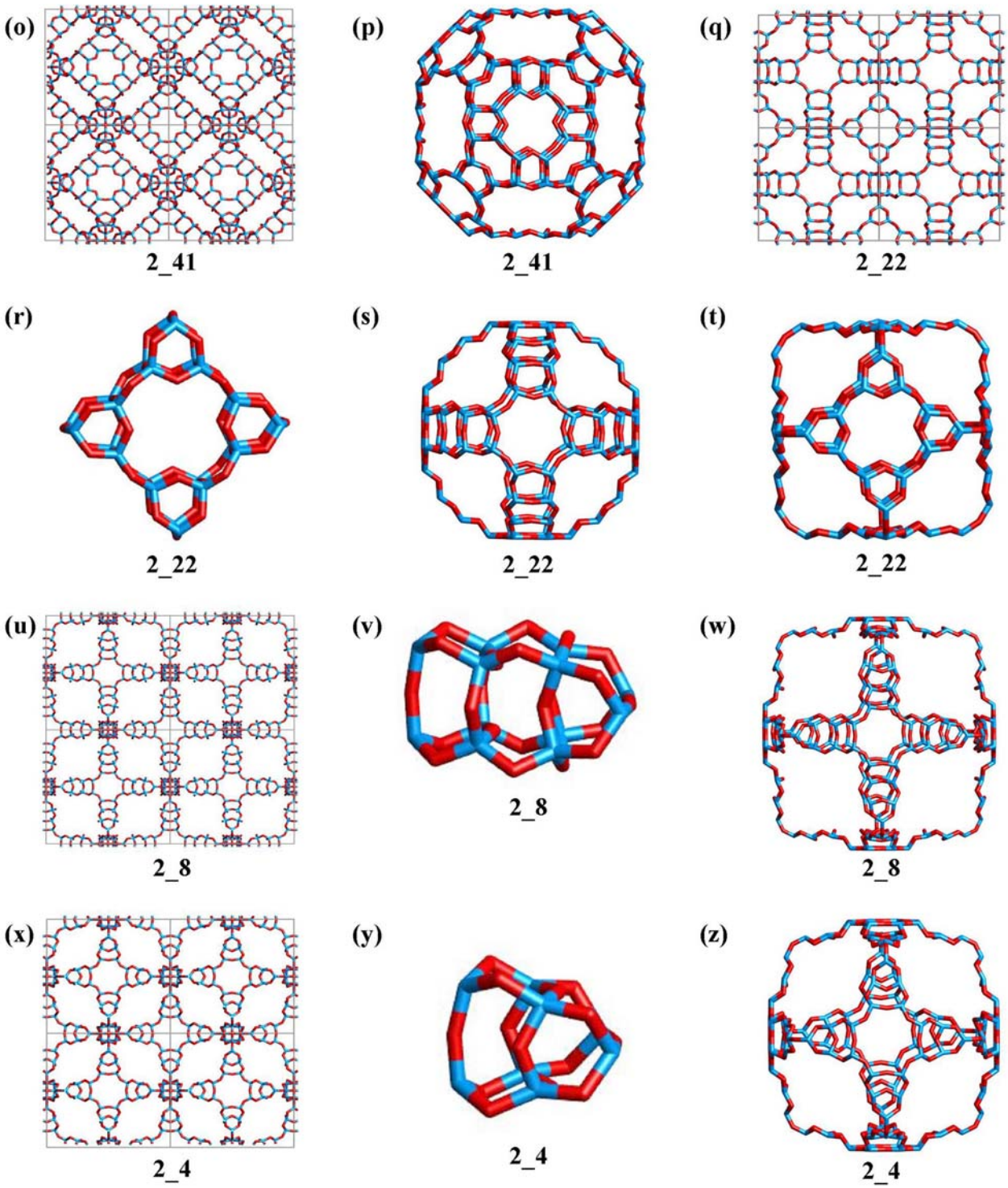

Figure 15. (Cont.)

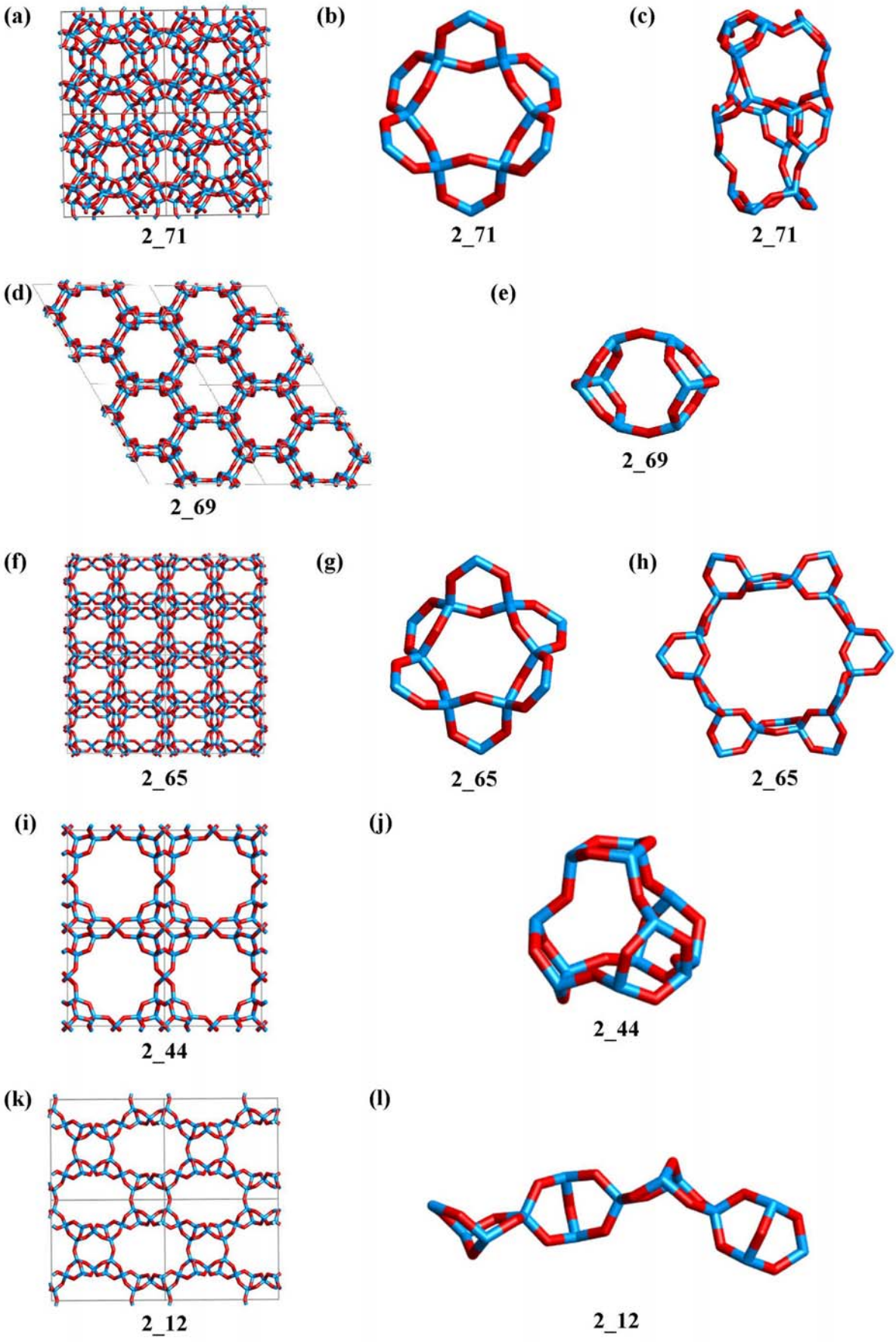

Figure 16. Molecular graphic illustrations of structures from the 3-ring family.

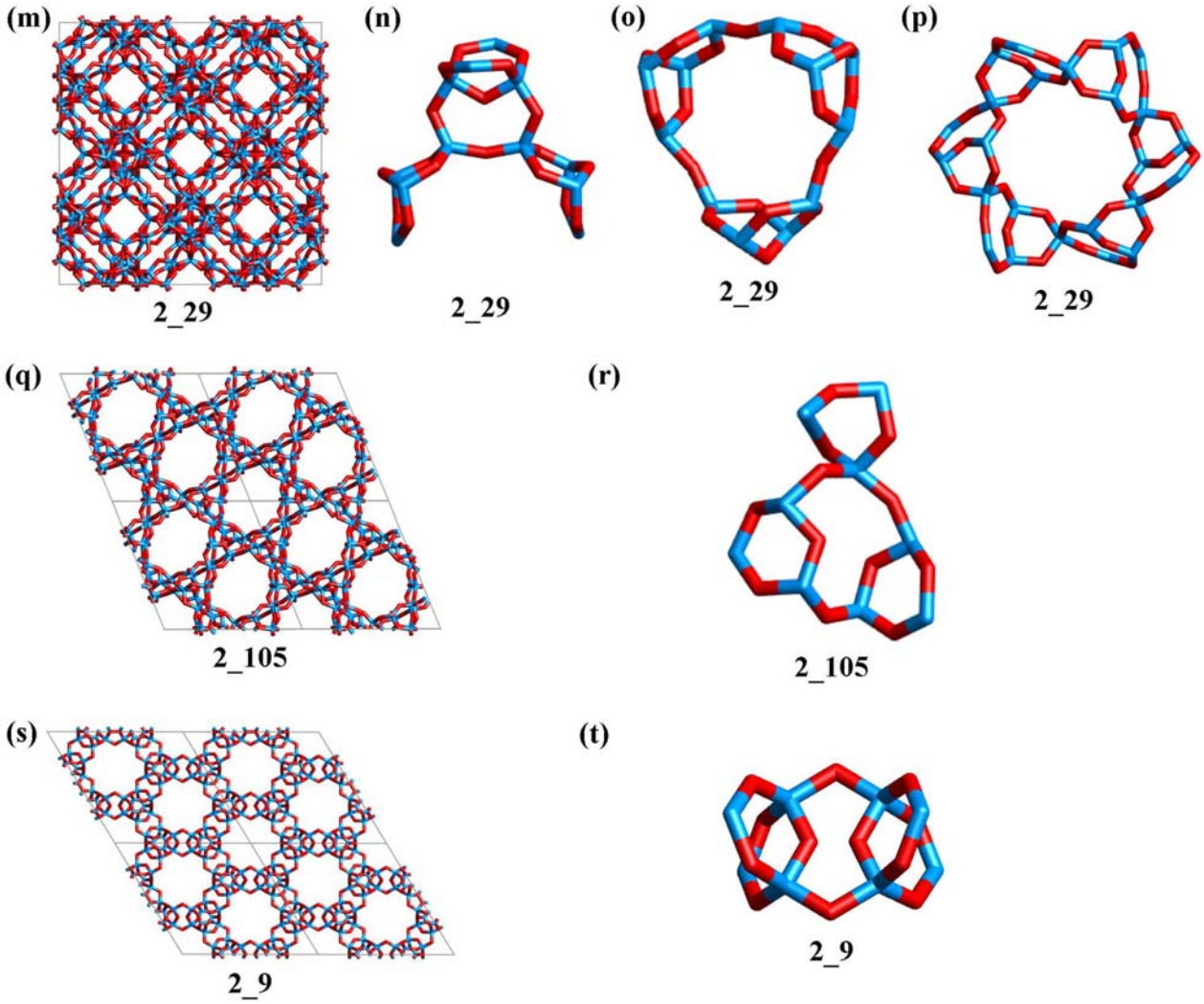

Figure 16. (Cont.)

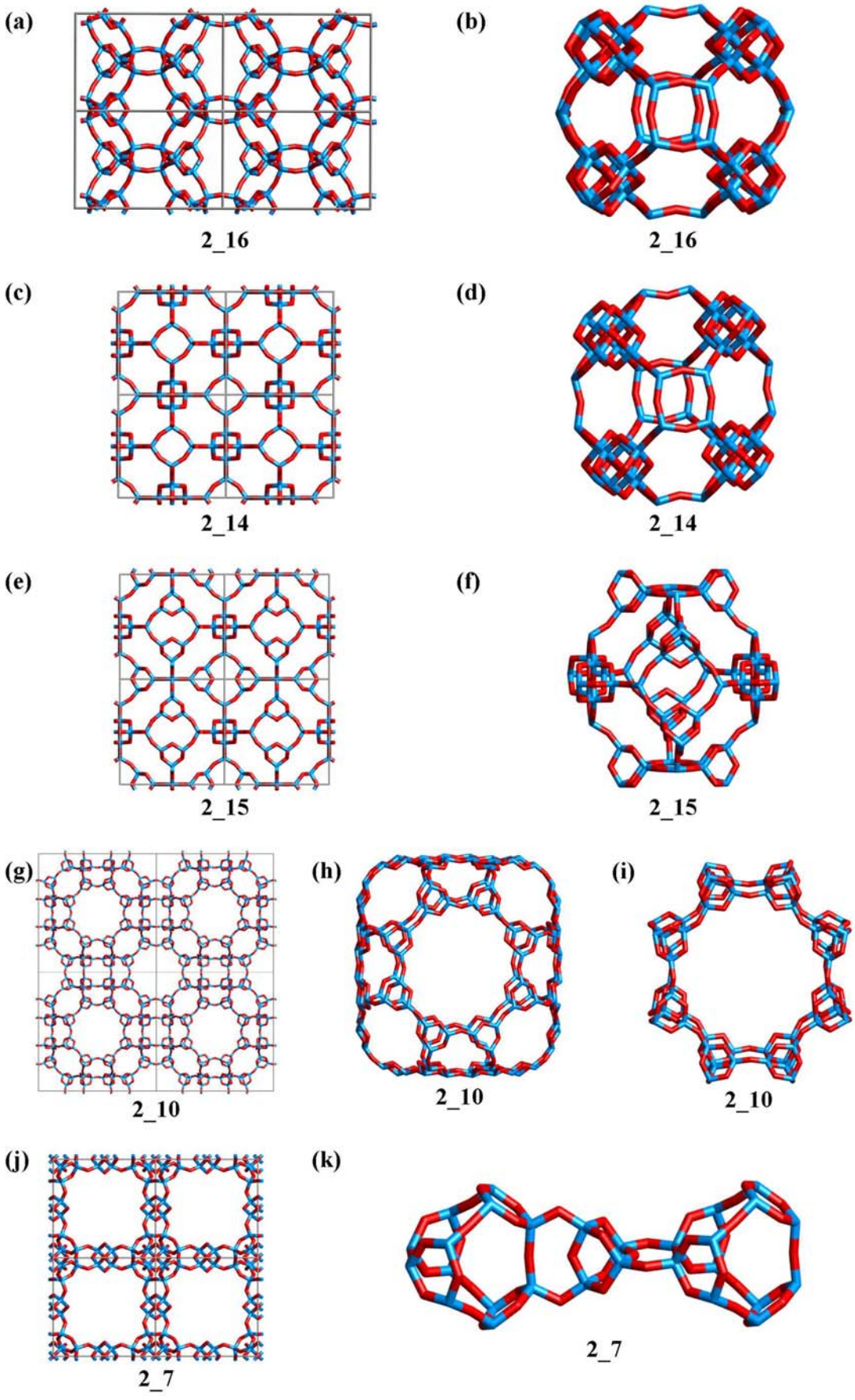

Figure 17. Molecular graphic illustrations of structures from the [3^4] family.

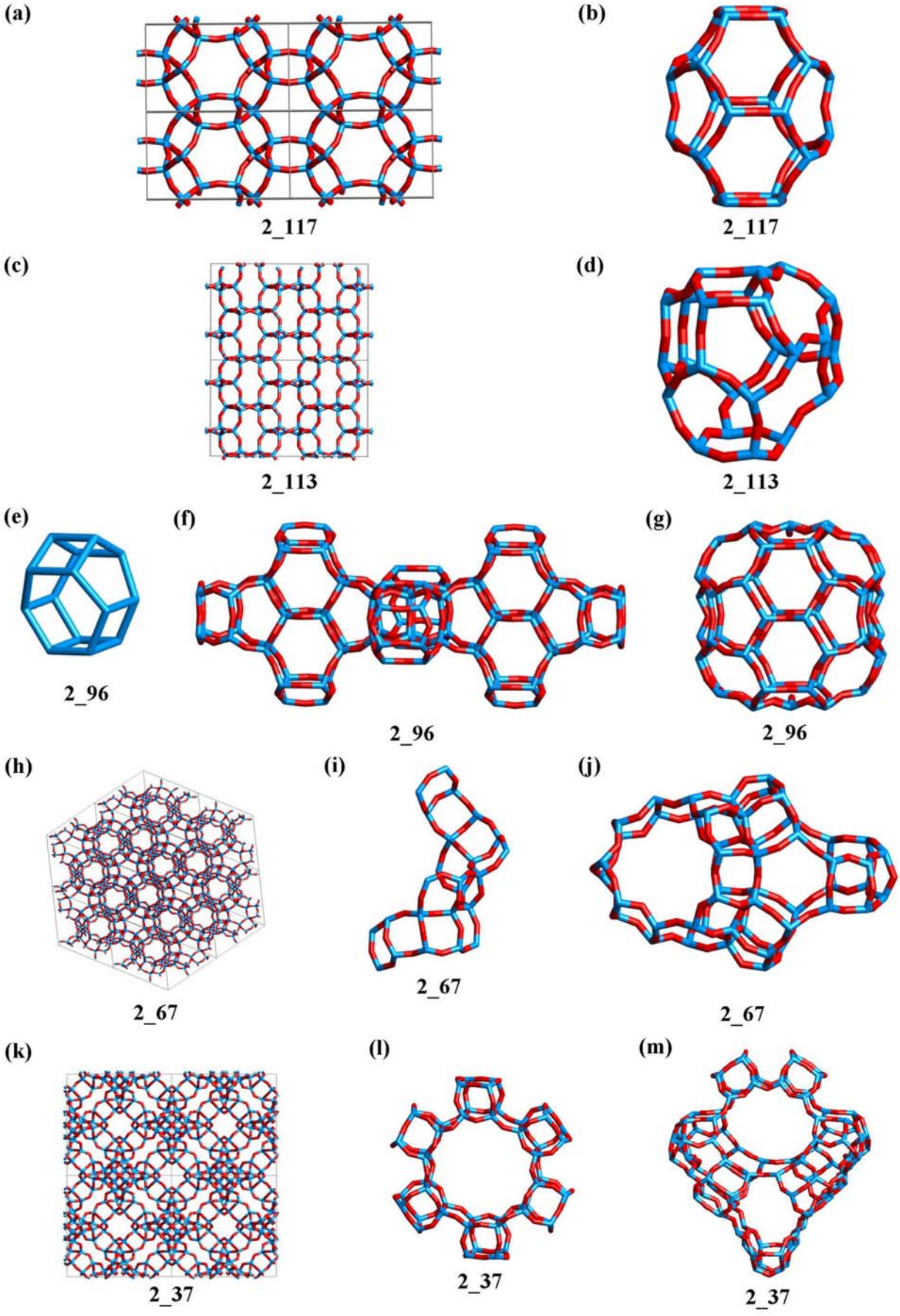

Figure 18. Molecular graphic illustrations of the Orphan structures.

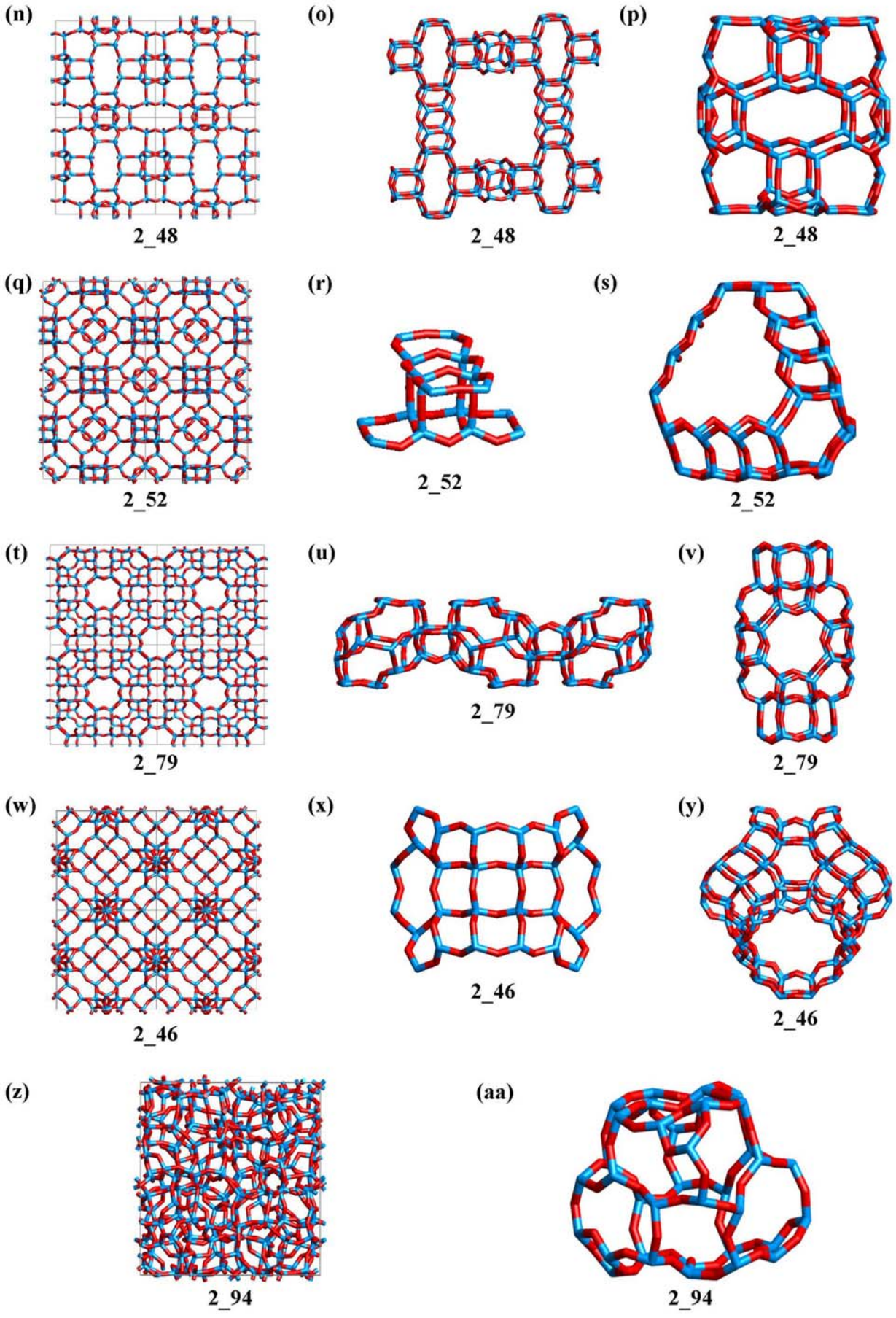

Figure 18. (Cont.)

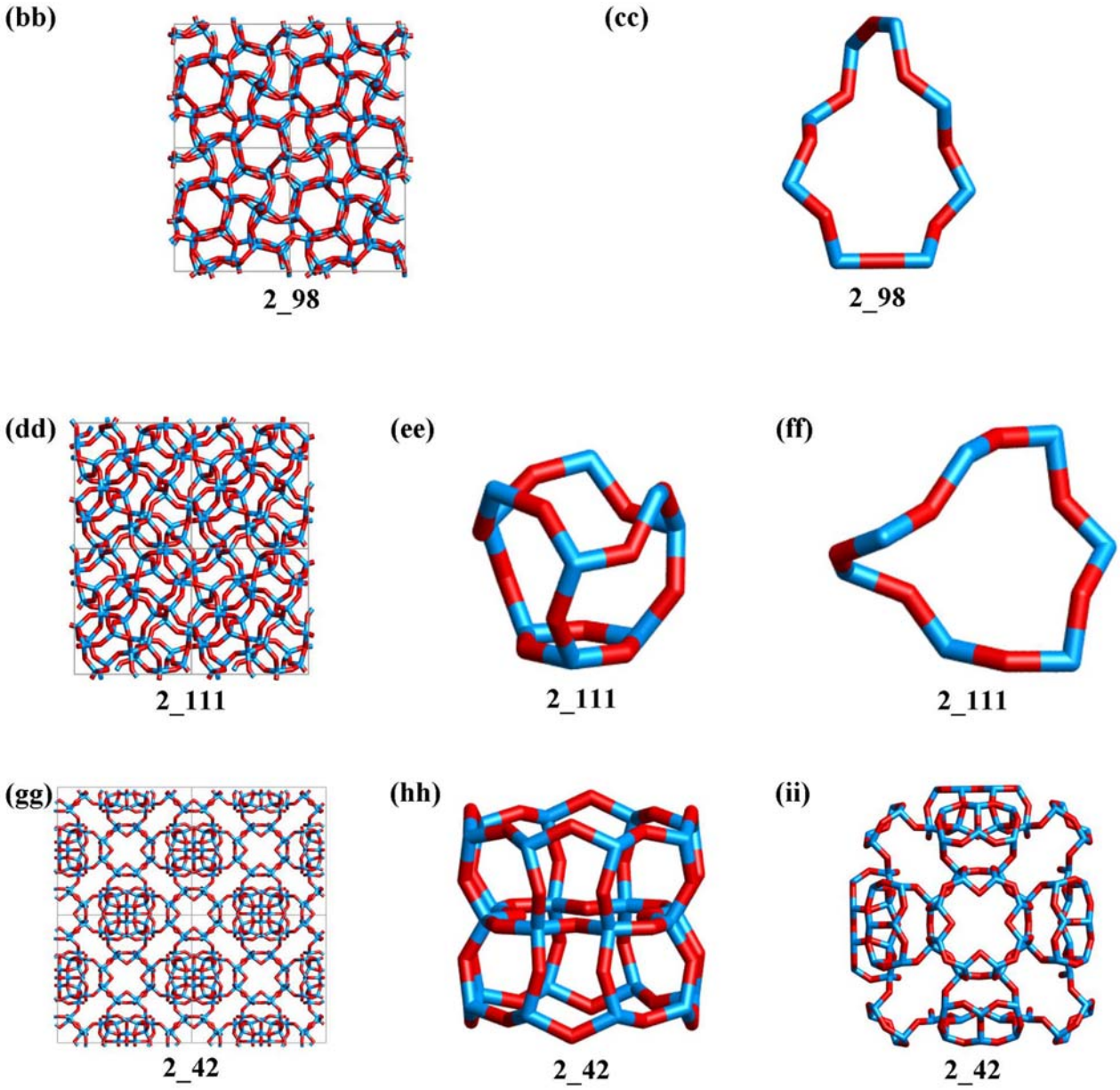

Figure 18. (Cont.)